Sub-Terahertz Channel Sounder: Review and Future Challenges

Lyu, Yejian; Kyösti, Pekka; Fan, Wei

Published in:
China Communications

Publication date:
2021

Document Version
Accepted author manuscript, peer reviewed version

Sub-Terahertz Channel Sounder: Review and Future Challenges

Yejian Lyu, Pekka Kyösti, and Wei Fan

***Abstract*—Due to the large amount of unused and unexplored spectrum resource, the so-called sub-Terahertz (sub-THz) frequency bands from 100 to 300 GHz are seen as promising bands for the next generation of wireless communication systems. Channel modeling at sub-THz bands is essential for the design and deployment of future wireless communication systems. Channel measurement is a widely adopted method to obtain the channel characteristics and to establish the mathematical channel models. Channel measurements depend on the design and construction of channel sounders. Thus, reliable channel sounding techniques and accurate channel measurements are required. In this paper, the requirements of an ideal channel sounder are discussed and the main channel sounding techniques are described for the sub-THz frequency bands. The state-of-the-art sub-THz channel sounders reported in the literature and respective channel measurements are presented. Moreover, a vector network analyzer (VNA) based channel sounder, which supports frequency bands from 220 to 330 GHz is presented and its performance capability and limitation are evaluated. This paper also discussed the challenge and future outlook of the sub-THz channel sounders and measurements.**

***Index Terms*—Radio propagation; Beyond 5G communication; Sub-Terahertz; Channel sounding techniques.**

I. Introduction

The commercialization of the fifth-generation (5G) communication has been carried out in recent years. However, the ever-increasing request for high data-rate has motivated the research for high frequency region where large frequency band is unused and unexplored. Though the borders of the Terahertz (THz) band are vaguely defined in the literature, it is commonly agreed to encompass radiation of 30 μm to 3 mm wavelength corresponding to frequency band from 100 GHz to 10 THz [1]–[3]. To avoid unnecessary conflicts with the THz definition, we call the lower end of the THz band i.e., 100 GHz to 300 GHz, the sub-THz band. In this work, sub-THz band is discussed thanks to its potential application in mobile communication for beyond 5G systems.

Surveys on frequency-dependent atmospheric absorption of electromagnetic waves in [4]–[7] provide an important guidance for selecting appropriate sub-THz frequency bands for wireless communication. The free space attenuation caused by atmospheric absorption at sub-THz frequency bands, especially at 120 and 183 GHz bands, is much higher than that at lower frequency bands. According to these surveys, 140 and 240 GHz frequency bands have less atmospheric attenuation compared to other sub-THz bands, and are suitable for long-range broadband communications [8]. Currently, many countries and organizations are concentrating on the studies at sub-THz frequency bands. In 2015, wireless applications and use cases in the frequency bands from 50 to 300 GHz were proposed by the European Telecommunication Standards Institute (ETSI) [9]. In 2017, IEEE 802.15.3d published the sub-THz wireless communication standard, which provided a new physical layer for high data rate wireless networks from 275 to 325 GHz with 8 different channel bandwidths from 2.16 up to 69.12 GHz [10]. The Federal Communication Commission (FCC) expanded spectrum licenses for the spectrum above 95 GHz in 2019 [11]. Moreover, the International Telecommunication Union (ITU) identified the frequency bands from 275 to 450 GHz for land mobile and fixed service applications in World Radiocommunication Conference 2019 (WRC-19) [12].

The wireless propagation channel is the physical medium through which radio-frequency (RF) signals are transmitted and the channel characteristics determine the ultimate performance limit of wireless communications [13]. Channel characteristics and models are a necessity for the design and deployment of wireless communication systems [14]–[17]. Channel measurement is a widely adopted method to obtain the channel properties and establish the channel models. The channel characteristics of interest include the large-scale properties, e.g., path loss (PL) and shadowing, and the small-scale characteristics, represented by the multi-dimensional dispersion of the channel, e.g. delay spread (DS), and the co- and cross-polarization characteristics [18]. At sub-THz bands, due to the wavelength approaching the size of dust and rain, etc., the behavior of the sub-THz channel might be different compared to the conventional low frequency spectrum [4], [19], [20]. Therefore, channel measurement campaigns at sub-THz bands need to be conducted and sub-THz channel characteristics and models should be investigated for the future communication systems.

The so-called "channel sounder" is a measurement device with the following functions: the transmitter (Tx) sends out a signal to excite the channel, the receiver (Rx) observes the output of the channel, and then the output is stored [13]. The channel impulse response (CIR) or one of the other system functions, e.g., the channel frequency response (CFR) in frequency domain channel sounder, can be obtained from the knowledge of the transmitted and received signals. Generally, based on sounding techniques, the channel sounders utilized in the literature can be categorized into two types, i.e., time domain sounder (e.g. impulse sounder [21], [22] and

Y. Lyu and W. Fan are with the Antennas, Propagation and Millimetre-Wave Systems (APMS) Section, Aalborg University, Aalborg 9220, Denmark.

P. Kyösti is with Oulu University and also with Keysight Technologies Finland Oy.

(Coresponding author: Wei Fan.)

correlation-based channel sounder [23], [24]) and frequency domain sounders (e.g. vector network analyzer (VNA) based channel sounder [25]–[27]) [28]–[30]. Detailed principles and architectures of channel sounders are described in Section III.

A reliable sub-THz channel sounding technique is the guarantee for obtaining accurate channel response data. However, to our best knowledge, there has been no review that thoroughly investigates the sub-THz channel sounding techniques. Thus, this work focuses on providing a review of the current channel sounding techniques and measurements at sub-THz frequency bands. The contributions of the study presented here are listed in the following:

1) Requirements of an ideal sounder are discussed. Based on these requirements, different state-of-art channel sounding techniques are introduced and compared.
2) Reviews of sub-THz channel sounders and channel measurements in terms of different channel sounding techniques are provided and discussed. Based on these reviews, the challenge and future outlook of the sub-THz channel sounder is provided and discussed.
3) A VNA based channel sounder from 220 to 330 GHz is presented, and the performance capability and limitation are evaluated. Furthermore, a double directional measurements are conducted in a laboratory scenario and the results are analyzed.

The rest of this paper is organized as follows. In Section II, requirements for an ideal channel sounder are discussed. Section III contains the current channel sounder techniques for sub-THz channel measurements. Section IV reviews the state-of-art sub-THz channel sounders, together with the sub-THz channel measurements and models. Section V outlines the architecture of the sub-THz channel sounder at 300 GHz. Section VI discusses the sub-THz challenge and future outlook. Finally, concluding remarks are addressed in Section VII.

II. Requirements and uniqueness of the sub-THz channel sounder

A. Requirements for the sub-THz channel sounding techniques

Channel sounding is a fundamental task for wireless communication engineering. To obtain the accurate channel model for wireless communication, an ideal channel sounder is desirable. Some key properties of an ideal channel sounder are discussed below:

- **Flexible carrier frequency setting.** The frequency allocation for the beyond 5G communication systems has not been fully determined yet. Besides, the frequency dependence of channel parameters is important and needs to be investigated and understood. Therefore, flexible carrier frequency settings are required to ensure that all potential sub-THz frequency band can be investigated.
- **Scalable system bandwidth.** According to the upcoming IEEE standard, future beyond 5G communication system will be an ultra-wideband (UWB) system [10]. For channel measurements, the bandwidth setting should be typically much wider than the true communication system. For example, the bandwidth of each carrier is up to 20 MHz in 4G communication systems, while hundreds MHz bandwidth is required for a channel sounder. Carrier aggregation scheme, where several frequency bands are aggregated to improve system data rate, are expected for future communication system as well. Therefore, scalable system bandwidth is desired to meet future system requirements.
- **High sampling rate.** Doppler frequency is a measure for the rate of change of the channel, and it is an important parameter for wireless communication system. The maximum Doppler shift is given by:

$$f_d = \frac{v}{\lambda} = f_c \cdot \frac{v}{c_0} \tag{1}$$

where f_d, λ, v, f_c, and c_0 denote the maximum Doppler frequency, the wavelength of the carrier frequency, the speed of the movement, the carrier frequency, and the speed of light, respectively. The Doppler frequency depends on the speed of moving object and the carrier frequency. According to the Nyquist sampling theory, the sampling rate of the sounder must be at least twice of the maximum Doppler frequency to avoid aliasing effects [31]. In sub-THz bands, the effect of the Doppler frequency will be more severe compared to the lower frequency bands, and therefore even small movements such as the movement of pedestrian should be taken into account in the sub-THz channel. Besides, clock errors cause artificial Doppler shift. Thus, the clock signals of the ideal sounder should be perfect.
- **High dynamic range.** The dynamic range is the power ratio between the maximum peak and the noise floor. It depends on the sounding principle and the particular hardware structures [32], which can directly affect the maximum detectable measurement distance. Due to the high atmospheric attenuation at the sub-THz frequencies, the dynamic range of the sub-THz channel sounder is more critical to ensure good signaling condition with a reasonable communication range. Applying high-gain power amplifiers, directional antennas and some new techniques e.g. the radio-over-fiber (RoF) techniques can significantly increase the dynamic range of sub-THz channel sounder, which however often imply high cost and more complicated system design.
- **Scalable measurement distance.** The supported channel measurement distance should be at least longer than the link distance in typical deployment scenarios. In outdoor scenarios, in order to investigate the large scale characteristics of sub-THz channel, i.e. PL and shadowing, the required distance might be up to several hundred meters. Even in some indoor scenarios, e.g. big shopping mall [33], the measurement distance can be quite large. An ideal channel sounder should meet the measurement distance requirements of all these scenarios.
- **Scalable antenna configuration.** Massive multiple-input multiple-output (MIMO) is a current research topic for its ability to achieve a better performance in wireless communication systems [34], [35]. Multiple antenna systems are widely adopted in commercial communication systems, and it is expected to be a key physical layer

technology. In channel measurements, MIMO measurements are also beneficial to obtain the spatial information of the channel. It is worth mentioning that the real MIMO configuration is complicated and costly, especially for massive MIMO system, and therefore virtual array concept has been widely adopted in the literature [36]–[38].

- **Size and flexibility of the device.** This requirement may be crucial for some application domains. For example, it may be necessary for the Tx or the Rx to be small and human portable in highly dynamic vehicular scenarios and channel measurement campaigns to understand near-field human body impact [32].
- **Cost effective.** A channel sounder is substantially more expensive compared to the actual communication devices. Besides, when the carrier frequency increases, the hardware requirements of the channel sounder become higher, which leads to a higher system cost.
- **Precision.** In an actual communication system, there are requirements of the radio performance, e.g., error vector magnitude (EVM), radio-frequency (RF) sensitivity. These requirements of a channel sounder (i.e. the measurement instrument) should be more demanding as compared to the expected communication system and its tranceivers.

Due to the hardware and cost limitations, practical channel sounders can not achieve all of the requirements of an ideal sounder. Depending on the channel sounder principle and structure, certain requirements can be met while others can not. In the next section, different types of the sub-THz channel sounder principle, structure and their pros and cons are introduced.

B. Sub-THz channel sounder uniqueness

In this subsection, the main differences among sub-THz, millimeter wave (mmwave) and microwave channel sounding techniques are discussed as follows:

- **Antennas.** Antennas are inherently incorporated in the channel sounding system. Practically speaking, the maximum directive gain or directivity of an antenna depends upon its physical size compared to wavelength. As the frequency goes up, the antennas can become more directive. For microwave and mmwave bands, both omnidirectional and directional antennas are employed for channel sounding purpose, while for sub-THz bands, the antennas employed are typically very directive. Omnidirectional antennas can be easily found, both for vertical and horizontal polarization at microwave bands. However, only vertically polarized omnidirectional antennas are available at mmwave bands. For example, validation of channel cross polarization ratio is still a problem in 3GPP Frequency Range 2 (FR2) MIMO over-the-air (OTA) due to lacking of horizontal polarized omnidirectional antennas [39]. Furthermore, due to the large antenna size (in terms of wavelength), the sub-THz antenna can be very directive and ultra-wideband, yet physically small.
- **Generation of high operation frequency.** For microwave bands, operating frequency can be easily realized with the signal generator and signal analyzer. However, it is getting more difficult as the frequency goes up. For mmwave bands, frequency mixer solution is often employed to save the system cost as well as to minimize the cable loss. For sub-THz bands, frequency extender solution needs to be employed since the sub-THz frequency is not directly supported (e.g. the maximum frequency supported by N5227B VNA is 67 GHz). Another strategy to generate sub-THz signal is to separate sub-THz signal from laser beam by using a DC bias, as introduced in Section III-B.
- **Channel sounder structure.** For microwave bands, channel sounder structure with massive parallel RF chains or switched RF chains are popular. Examples of channel sounder systems include [32], [40], [41] with 56×32, 128×16, and 128 element arrays at 2.6 and 3.5 GHz. For mmwave bands, due to the high system cost and hardware limitation, the RF chains of the channel sounder are limited, e.g., [42], [43] with 8 and 16 parallel chains operating at the frequencies of 21.5 and 83.5 GHz, respectively. One exception is the 28 switched GHz massive MIMO system with 256×128 element arrays in [44]. For sub-THz channel sounder, one chain at the Tx and the Rx side are typically employed at the moment for channel sounding.
- **Delay resolution.** At sub-THz bands, the operating bandwidth can be ultrawide (e.g. 110 GHz in our channel sounder), compared to microwave bands (e.g. 200 MHz in [32]) and mmwave bands (e.g. 5 GHz in [45]). Consequently, this UWB can provide a high delay resolution of approximately 3 mm in propagation distance. This new feature enables identification of more precise propagation paths, which is not possible for the lower frequency bands.
- **Measurement distance.** Signal transmission loss and cable loss are the main influencing factors for the maximum measurement distance that channel sounders can achieve. For microwave bands, the signal transmission loss and cable loss are low. Therefore, the measurement distance can be up to tens of kilometers, e.g., 45 km at 2 GHz in [46]. For mmwave bands, the transmission loss and cable loss are severe compared to those of microwave bands, which results in the measurement distance being reduced to hundreds of meters, e.g., 685 m at 83.5 GHz in [45]. High signal transmission loss and cable loss become the main problems of sub-THz channel propagation, which result in shorter link distance in channel measurements, e.g., several tens of meters. However, with the application of RoF techniques to reduce the cable loss, the measurement distance can reach 100 m [47].
- **Phase measurements.** Phase is getting more sensitive as the frequency goes up, which makes accurate phase measurement more difficult. Virtual array concept, which uses one antenna sequentially in many pre-defined spatial locations for channel spatial domain measurements, is a mature technology for microwave and mmwave

bands [48], [49]. However, no results have been reported for sub-THz bands, due to lacking of accurate phase measurement introduced by errors in system, e.g. cable moving and bending. Furthermore, synchronization will be more difficult for sub-THz channel sounder.

III. Sub-THz channel sounder and directional measurements principle

Channel sounder with signal generator and spectrum analyzer, THz Time Domain Spectroscopy (THz-TDS), VNA based channel sounder, and correlation-based channel sounder are the four main channel sounding techniques in THz frequency bands. According to the sounding technique classifications in Section I, these channel sounding techniques can be classified into time domain (i.e., THz-TDS and correlation-based channel sounder) and frequency domain (i.e., channel sounder with signal generator and spectrum analyzer and VNA based channel sounder). The principle and structures of these channel sounders are introduced as follows. Moreover, review of the state-of-the-art channel sounders are listed and summarized. Comparison of these four channel sounder and summaries of the state-of-the-art sub-THz channel sounders are illustrated in Table I and II, respectively.

A. Channel sounder with signal generator and spectrum analyzer

This is the simplest and most straightforward setup to measure the power based channel parameters. Signals are generated from the signal generator (SG) and modulated to THz bands at the Tx side. At the Rx side, the received signals are demodulated and stored in the spectrum analyzer (SA). Although the cost and complexity of this sounder is low compared with the other three sounders, it can only conduct power-based measurements and thus not detailed in the following. The power based response $PL(f)$ at a certain frequency f can be obtained [55]:

$$PL(f) = \frac{P_R(f)}{P_T(f)} \tag{2}$$

where $P_T(f)$ and $P_R(f)$ represent the transmitted power and the received power.

B. THz Time Domain Spectroscopy

The structure of the THz-TDS is demonstrated in Fig. 1. A typical THz-TDS consists of five components: a femtosecond laser, a beamsplitter (BS), a THz transmitter, a mechanical delay line and a THz detector [56]. A known short laser pulse is sent to the BS and then it is split into two beams. One beam is directed to the THz transmitter. DC bias is used to separate the optical carrier and the THz pulse, and then the THz pulse is emitted. The other beam is routed through the mechanical delay line to the THz detector at the Rx side. Mechanical delay line is computer-controlled micron-level positioning stage to obtain the time delay τ. Note that only when the laser pulse and the THz signal arrive simultaneously, the THz detector will be activated to receive the THz signal. Therefore, each

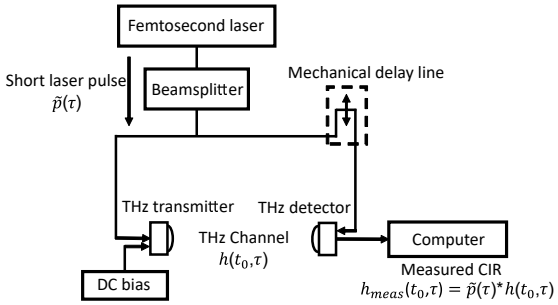

Fig. 1: A schematic diagram of a typical THz-TDS.

length step of the mechanical delay line is scanned until the THz detector is activated, and the delay τ can be obtained by calculating the length of the delay line. The delay changes 6.6 fs for each micrometer of the delay line displacement [57]. The moving speed of the delay line (i.e., picosecond level) defines the sampling rate of the THz-TDS. Firstly, we define a channel snapshot as the practical implementation of a CIR. The measured CIR $h_{mea}(t_0, \tau)$ for a given channel snapshot t_0 can be written as:

$$h_{mea}(t_0, \tau) = \widetilde{p}(\tau) * h(t_0, \tau) \tag{3}$$

where $\widetilde{p}(\tau)$ and $h(t_0, \tau)$ represent the sounder impulse response and the true CIR. Since the optical pulse is significantly shorter than the THz pulse, the sounder impulse response $\widetilde{p}(\tau)$ can be closer to a Delta function, and the measured CIR $h_{mea}(t_0, \tau)$ is more approximate to the true CIR $h(t_0, \tau)$.

THz-TDS has the advantages of huge and scalable bandwidth at THz frequencies [58]. However, due to the large size of a spectrometer and the limited output power, it is not suitable for the channel measurements over a link distance of few meters [19]. The THz-TDS is usually used for channel measurements in a small distance range and material measurements of electrical and scattering parameters.

C. Vector Network Analyzer based channel sounder

VNA has been widely used in channel measurements [27], [36], [59]–[61] and it is one of the most popular measurement device in frequency domain sounding techniques due to its ability to perform a frequency sweep over a large bandwidth, ease of calibration, and ease of access in RF laboratory [62]–[65]. Conventionally, two-port VNAs are commonly used for low frequency channel measurements [36], [66], e.g., centimeter-wave band. The schematic disgram of the two-port VNA is illustrated in Fig. 2 (a). The VNA can measure the complex scattering parameter S_{21} by sending sinusoid signals from port one and sweeping discrete narrowband frequency tones across the bandwidth of interest from port two [13]. The relationship between S_{21} and the frequency response $H(f)$ is demonstrated as:

$$S_{21}(f) = H_{system\_Tx}(f) H_{Tx}(f) H(f) H_{Rx}(f) H_{system\_Rx}(f) \tag{4}$$

where f denotes the frequency, $H_{system\_Tx}(f)$, $H_{Tx}(f)$, $H_{Rx}(f)$, and $H_{system\_Rx}(f)$ represent the response of the

TABLE I: Comparison of the channel sounders based on requirements.

	Sounder type			
	SG and SA	THz-TDS	VNA-based	Correlation-based
Pros	The carrier frequency is flexible, however, it might require multiple frequency extenders.	The carrier frequency is flexible.	The carrier frequency is flexible, however, it might require multiple frequency extenders.	The carrier frequency is flexible, however, it might require multiple frequency extenders.
	The measurement distance could reach to dozens of meters.	Extremely high bandwidth, e.g. several THz [50].	High bandwidth, e.g. 110 GHz [51].	High sampling rate and could be used in dynamic scenario.
	It is cost-effective compared to other three sounders.	High sampling rate.	High dynamic range and with RoF techniques the dynamic range could reach to 130-140 dB [33], [47].	High dynamic range, e.g. 145 dB [8].
			The measurement distance could reach to dozens of meters, and it could reach to 100 meters with RoF techniques at 140 GHz [47].	The measurement distance could reach to dozens of meters.
			With virtual array condition, it could fulfill the requirement of scalable antenna configuration, e.g. [52].	The sounder could achieve scalable antenna configuration, e.g. the sounder achieves 2×2 MIMO system at 300 GHz in [53].
Cons	Only for power-based measurements.	Low dynamic range.	High signal loss in the cable.	Smaller bandwidth compared to VNA-based sounder and THz-TDS.
	Complex synchronization in long-range measurements.	Short measurement distance, e.g. a few tens of centimeters [54].	Sweep time determined by IF bandwidth setting and frequency points.	Complex synchronization in long-range measurements.
		Large size of the spectrometer.	High cost of the VNA and frequency extenders.	Complex design, additional hardware and high cost.

system at the Tx side, the Tx antenna, the Rx antenna, and the system at the Rx side, respectively.

After calibrating the system response, the frequency response with the response of antennas $H_{Tx}(f)H(f)H_{Rx}(f)$ can be obtained. The CIR $h(\tau)$ can be obtained by applying an inverse discrete Fourier transform to the calibrated frequency response. A wide bandwidth can be set for the channel measurements and a high dynamic range can be realized by the post-processing to reduce random noise by averaging or applying amplifier at the Tx or Rx side. On the downside, the channel is required to be static when the VNA sweeps the band of interest, since frequency sweeping operation is generally slow, e.g, 9.2 s for one sweeping operation for 1 kHz IF bandwidth and 10001 frequency points. Thus, VNA based channel sounder is not suitable for the channel measurements in highly dynamic scenarios.

At mmwave bands and sub-THz bands, four-ports VNAs and frequency extenders are used [27], [59]–[61], [67]–[73]. The additional ports can be used to generate a local oscillator signal for the mixer in the frequency extension in order to elevate the VNA original frequencies to much higher frequencies [19], as shown in Fig. 2 (b). The channel sounder can be separated into two parts: transmitting port and receiving port. On the transmitting port side, VNA generates intermediate frequency (IF) signal, e.g. 10 GHz. Then the signal is amplified by an amplifier (AMP) and modulated with a N times multipled local oscillator (LO) signal to THz bands. Moreover, the signal is filtered by a band-pass filter (BPF) and transmitted by the Tx antenna. On the receiver side, the received signal is firstly amplified by the low noise amplifier (LNA) and then demodulated with the same LO signal splitted from the VNA port three, and finally stored in the computer. In channel measurements, the Tx and the Rx require cable connection with the VNA in order to remote the antenna and synchronize the phase. The signal attenuation in the coaxial cable increases as the frequency increases [74]. Thus, the cable connections between the Tx, the VNA and the Rx cause high cable loss and reduce the dynamic range. Consequently, the reduced dynamic range leads to short measurement range.

To combat the problem of high cable loss, currently, the RoF techniques are applied in the VNA based systems [75]–[77], in which the electrical-to-optical (E/O), the optical-to-electrical (O/E), and the optical fiber cables are used, as depicted in Fig. 2 (c). The Tx and Rx extenders are the same as the former VNA system. After demodulated by the Rx extender, the signal is converted to the optical signal by the E/O unit and transmitted through the optical fiber. Then the signal is converted back to the IF band and sent to the VNA. The transmission loss through the optical fiber is much lower than the loss through the coaxial cable, e.g. 0.4 dB/km for a single-mode optical fiber [78] and approximately 1.59 dB/m for a coaxial cable at 30 GHz [62]. The use of RoF techniques can significantly increase the dynamic range of the system to 140 dB, and the measurement range can reach 100 meters [33], [47]. However, due to the thermal and mechanical stresses, the fiber cables are sensitive to phase change [79], [80], which

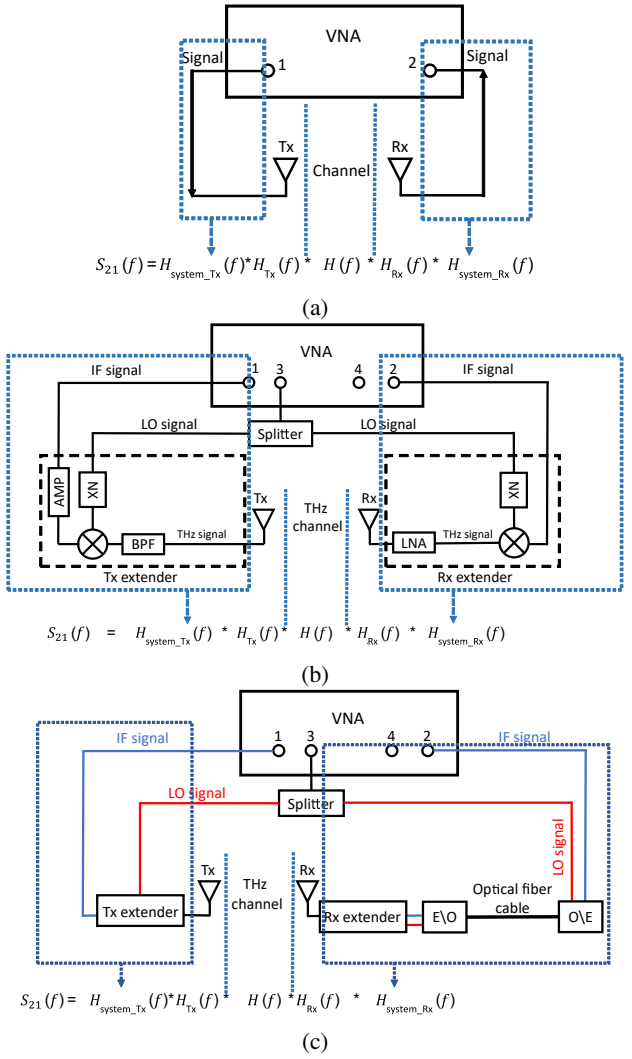

Fig. 2: The schematic diagrams of VNA based channel sounder. (a) Two-port VNA based channel sounder; (b) Four-port VNA based channel sounder with frequency extender; (c) VNA based channel sounder using RoF techniques.

indicates that the RoF techniques are not suitable for the phase measurements and have typically been applied in power measurement. A phase-compensation scheme proposed in [62] can be used to combat the random phase change in the optical fiber.

D. Correlation-based channel sounder

Correlation-based channel sounder is a popular time domain sounder due to their simple implementation and applicability in different sounding scenarios [23], [24], [81]–[84].

The principle of the correlation-based channel sounder is as follow: A known maximal-length pseudo-random binary sequences, alternatively known as pseudo-random noise (PN) sequence is transmitted over a channel, the received signal $r(t_0, \tau)$ for a given channel snapshot t_0 can be written as

$$r(t_0, \tau) = h(t_0, \tau) * p_{Tx}(\tau) \tag{5}$$

where τ is the time delay variable, and $p_{Tx}(\tau)$ and $h(t_0, \tau)$ represent the PN sequence and the CIR, respectively.
On the receiver side, the received signal is cross-correlated with the identical and complex conjugated PN sequence $p^*_{Tx}(\tau)$. Thus, the resultant $s(t_0, \tau)$ can be written as:

$$\begin{aligned} s(t_0, \tau) &= r(t_0, \tau) * p^*_{Tx}(\tau) \\ &= P(\tau) * h(t_0, \tau) \end{aligned} \tag{6}$$

Since the auto-correlation function $P(\tau)$ of the PN sequence is a good approximation to the Dirac delta function, the resultant $s(t_0, \tau)$ is approximate to the CIR $h(t_0, \tau)$ [13], [85], [86].

A setup of the correlation-based channel sounder with frequency extender is illustrated in Fig. 3 (a). In a correlation-based channel sounder, a known PN sequence is first modulated by an IF signal and amplified, then mixed up with the local oscillator signal into the frequency range of interest, then the signal passes through the BPF. After being amplified by a power amplifier, the signal is radiated through the Tx antenna. At the Rx side, the received signal is down converted and amplified by a LNA, then is demodulated with the IF signal to the baseband. The demodulated signal is correlated with an identical PN sequence, and then the channel response is obtained [19]. The signals are sampled by an analog-to-digital converter (ADC) and the data can be processed by an Field-programmable gate array (FPGA) or stored in a computer for post-processing. According to Sampling Theory, to properly digitize the received signal, the sampling rate of the ADC must be at least twice the signal rate. For the narrowband channel measurements, this can be ignored. However, for the wideband channel measurements, especially for the UWB channel measurements at THz frequencies, the signal rate increases. Therefore, the system requires higher speed ADC, which will lead to higher cost and complexity [87].

In order to ease the hardware requirements for the wideband channel measurements, sliding correlation (SC) techniques are utilized [87], [88]. Unlike the correlation-based channel sounder using two identical PN sequence for autocorrelation, the sliding correlator uses two similar signals, where the PN sequence used at the Rx side is identical but at a slightly offset rate compared to the one used at the Tx side [87]. Multiplying these two similar signals together and carefully filtering their product will yield a very close approximation to a time-dilated autocorrelation. The schematic diagram of the SC-based channel sounder is depicted in Fig. 3 (b). After being sliding correlated, the signal is filtered by the low-pass filter (LPF) and then sampled by ADC. Currently, sliding correlators can offer 1 Gb/s baseband spread spectrum sequences, and generally enable cable-free operation over mobile communication distances of up to 200 meters at sub-THz frequencies [19], [28]. Since the SC-based channel sounder can record several hundred channel snapshots per second depending on the selected slide factor, which is much faster than the VNA based channel sounder, it can be utilized in a wider range of scenarios. Compared with VNA-based channel sounder, without the limitation of the cable connection, the dynamic range of the SC-based channel sounder can be higher, however, the complicated synchronization issuse between the

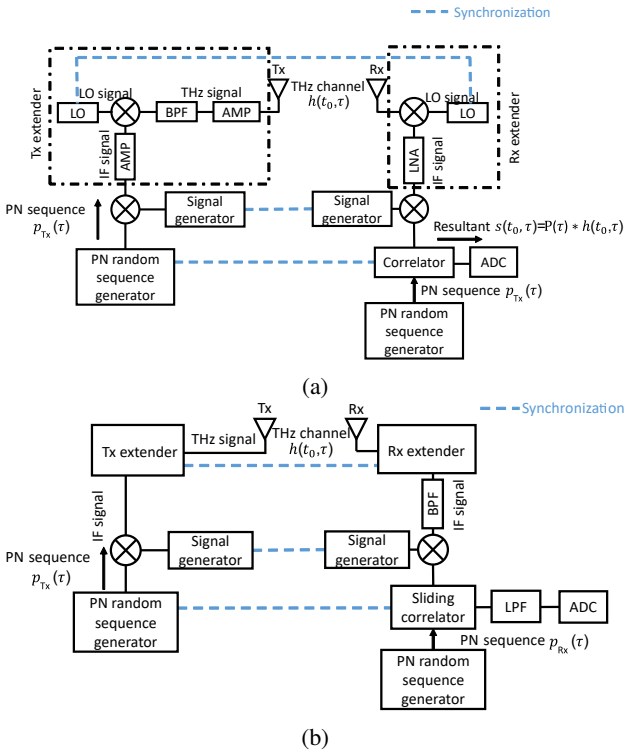

Fig. 3: The schematic diagrams of correlation-based channel sounder. (a) A simple correlation-based channel sounder with frequency extender; (b) SC-based channel sounder.

Tx side and the Rx side should be considered in the long distance measurements. On the other hand, the SC-based channel sounder has the smaller bandwidth and requires a more complex system design and additional hardware [28].

E. Channel spatial profile measurement

Directional scanning method and multi-antenna method are two basic directional measurement methods to obtain spatial domain channel characteristics.

1) Directional scanning method [27], [33], [47], [91]: In this method, highly directional antennas, which can be mechanically rotated, are applied at the Tx or the Rx or both. When the antenna rotates, the channel response at a specific direction can be obtained. By stepping different values of angles in azimuth and elevation, we can obtain an approximation of the channel response. This method requires the channel to be static during a total measurement duration, which encompasses the measurements of all the different angles [13]. The total measurement duration is long as the antenna has to be mechanically rotated to obtain the spatial channel response in all directions. Furthermore, the antenna patterns are inherently embedded in the channel measurements.
2) Multi-antenna method: This method can be categorized into three different approaches, i.e., real arrays, multiplexed arrays, and virtual array.
   - Real arrays method [41]: In this method, antenna arrays are applied at the Tx or the Rx, and the channel response is measured at all these antenna elements simultaneously. However, this method requires an individual RF chain for each antenna element, resulting in high system cost and complicated calibration.
   - Multiplexed arrays method [92], [93]: Multiple directive antennas are applied in this methods, however, it only requires one RF branch. This method uses a fast RF switch to change the connection from one directive antenna to another.
   - Virtual array method [37], [49]: This method uses only one antenna, which is mechanically moved from one position to the next, and we can measure the channel response per position (i.e. virtual array element). Compared with the other two antenna array methods, this is a cheap method with flexible antenna configuration and easy calibration and maintenance. However, this method is based on the assumption that the channel is static during the measurement and it often requires a long measurement time.

   After the measurement, the directional channel response can be extracted by high resolution parameter estimation (HRPE) algorithms e.g. Multiple Signal Classification (MUSIC) [94] and Space Alternating Generalized Expectation maximization (SAGE) [95].

At sub-THz bands, in order to combat the high atmospheric attenuation of the sub-THz bands, antennas with high gain and narrow beamwidth need to be applied with the channel sounding systems [19], [96]. Due to the hardware and cost limitation, most of the literature conduct the directional measurements by applying the directional scanning method [33], [47], [97]. As for the HRPE algorithm at sub-THz bands, mainly the spatial domain aspects, the accuracy is determined by the phase measurement accuracy and the robustness for the multiple RF channels in the multi-antenna channel sounder. However, this has become particularly challenging for the existing sub-THz channel sounder. Besides, due to the use of the high gain and narrow beamwidth antennas, the existing HRPE multi-antenna algorithms are not suitable for sub-THz bands

F. Synchronization method

Time and frequency synchronization is essential in channel measurements to ensure the CIR or CFR is recorded accurately. The time synchronization is used to simultaneously trigger the Tx and Rx operations, and the frequency synchronization eliminates the frequency offset of the local oscillators, enabling carrier phase measurements [98]. THz-TDS and VNA-based channel sounder are capable for synchronization, since the THz-TDS and VNA require cable connections between the Tx and Rx. However, the cable connections limit the channel sounder use to short-range measurements. As for other channel sounders, the conventional method for synchronization is to share the clock through 10 MHz reference cables between

TABLE II: Recent sub-THz channel sounder studies.

Reference	Frequency range (GHz)	Bandwidth (GHz)	Frequency/time domain	Equipment	Dynamic range (dB)
[50]	300-2000	1700	Time domain	THz-TDS	40
[89]	-	1100	Time domain	THz-TDS	48
[90]	100-15000	14900	Time domain	THz-TDS	-
[59]	300-310	10	Frequency domain	VNA	85
[68]	260-340	80	Frequency domain	VNA	60
[69]	275-325	50	Frequency domain	VNA	65
[70]	126-156	30	Frequency domain	VNA	105
[61]	110-170	60	Frequency domain	VNA	90
[47]	140-220	80	Frequency domain	VNA with RoF	140
[33]	141.1-145.1	4	Frequency domain	VNA with RoF	130
[8]	138-142	4	Time domain	SC	145
[53]	296-304	8	Time domain	Correlation-based	60

the Tx and Rx [53], which also lead to the limitation of the sounder use in vehicular-to-vehicular and long-range measurements. Another synchronization method is to use two separate, highly stable clocks, such as Rubidium (Rb) clocks, on the Tx and Rx sides [99], [100]. Compared to the conventional cheap crystal oscillators, Rb standard clocks have lower phase noise, long-term stability, and holdover capabilities [28]. However, the two Rb clocks require a back-to-back synchronization for a long time, e.g. several hours, before measurements.

G. Review on sub-THz channel sounders

THz-TDS sounding systems were presented in [50], [89], [90], [101], where flexible frequency settings of the THz-TDS from several hundred GHz to even 15 THz and the extremely wide system bandwidth were exhibited. However, the low dynamic range (e.g., less than 50 dB) and the large size of the spectrometer limit the measurement scenarios.

In the VNA based channel sounder part, VNA based channel sounders at sub-THz bands were presented in [59], [61], [68], [69]. The dynamic ranges of these sounders vary from 60 to 90 dB. However, due to the signal loss on the RF cables, the maximum measurement distance of these sounders are limited to several tens meters. In [33], [47], VNA based sub-THz channel sounders using RoF techniques were proposed. With the RoF techniques, the use of the optical fiber significantly increases the dynamic range and enables the measurement distance to exceed 100 meters.

Regarding the correlation-based channel sounder, a 300 GHz correlation-based channel sounder with 8 GHz bandwidth and a dynamic range of 60 dB was presented and evaluated in [53]. The hardware of this channel sounder allows it to support MIMO measurements up to 2×2 at 60 GHz and at 300 GHz. A SC-based channel sounder at 140 GHz with 4 GHz bandwidth and 145 dB dynamic range was proposed in [8] and has been used in indoor channel measurements. Although the measurement distance of correlation-based channel sounder can reach several ten meters, the system bandwidth is lower compared to the other two types of sounders.

IV. Review on sub-THz hardware development and channel measurements

In the former parts, the principles and structures of the channel sounders are illustrated and discussed. Until now, many efforts have been made in the sub-THz channel sounding techniques and measurements. In this part, the state-of-the-art technologies of the RF hardware and channel measurements at sub-THz bands are listed and summarized. However, this review is by no means a complete one and only some representative hardware and channel measurements are included in this work. In Table III, summaries of the sub-THz channel measurements are provided.

A. Review on sub-THz hardware development

To combat the high PL at sub-THz frequency range, high-gain antennas are required. In general, increasing the antenna aperture can achieve a high-gain sub-THz antenna. Dielectric lens antenna and phased array are the two main approaches to obtain a large aperture [1]. For the dielectric lens antennas, a lens is a specially shaped piece of dielectric material that has focusing and capability to improve the performance of the THz antennas, e.g., achieving good directivity and high gain [105]. The antenna gain depends on the size, shape, and dielectric properties of the lens. The maximum gains of the dielectric lens antennas achieved in [106], [107] are over 30 dBi at 300 GHz. Phased array has been widely adopted at mmwave frequency bands. Moving from mmwave bands to sub-THz bands, due to short wavelength, the number of array elements increases dramatically for the same aperture, which increases the system cost and complexity. In [108], the first 300 GHz phased array with 4 horn antenna elements was presented and the array gain was 20.7 dBi.

Power amplifiers and LNAs play important roles in transmitter and receiver designs, respectively. Their specific properties determine the ultimate limits for the achievable link range with highly frequency-dependent power delivery and noise properties [3]. The complementary metal oxide semiconductor (CMOS) technologies are widely adopted in the radio transceiver solutions for current 4G and 5G mobile terminals. However, these technologies are limited in power generation and efficiency above 140 GHz [1]. As a consequent, III-V technologies, e.g. gallium arsenide (GaAs) and silicon germanium (SiGe), are utilized to overcome the limitation of CMOS for the power amplifiers and LNAs at sub-THz bands. The state-of-the-art power amplifiers presented in [109]–[111] demonstrated the amplifiers can providing more than 17 dBm output power and more than 16% peak efficiency. For LNAs, the reported noise figure (NF) of the receivers or LNAs were in the range of $6-9.7$ dB from 120 to 170 GHz and 9.5 dB at 240 GHz [112]–[114].

TABLE III: Recent sub-THz channel measurement studies.

Reference	Frequency (GHz)	Equipment	Rotation	Measurement features
Material measurements				
[89]	100-500	THz-TDS	×	Reflection properties.
[101]	100-350	THz-TDS	×	Absorption and reflection properties.
[102]	100-1000	THz-TDS	×	Reflection and scattering properties.
[19]	138-142	SC	×	Penetration loss and scattering properties.
Indoor channel measurements				
[103]	350 & 650	SG and SA	×	PL and Reflection loss.
[59]	300-310	VNA	×	Channel transfer functions (CTF) and PL.
[68]	260-400	VNA	×	CTF, PL and absorption coefficient of materials.
[60]	240-300	VNA	×	PL
[61]	110-170	VNA	×	PL, shadowing, DS, and coherence bandwidth.
[69]	275-325	VNA	Rx directional	K-factors, DSs, and ASs; RT simulation.
[70]	126-156	VNA	×	PL, DS, AS, cluster.
[71]	140-220	VNA	×	PL
[73]	110-170 and 300-316	VNA	×	PL
[33]	141.1-145.1	VNA with RoF	Rx directional	PL, DS, and AS.
[52]	300-312	VNA	×	PL, shadowing, DS and Doppler shift of MIMO.
[8]	138-142	SC	Double directional	PL and penetration loss.
[97]	300-308	Correlation-based	Double directional	Power angle spectrum.
[104]	300-308	Correlation-based	Double directional	PL, DS, AS and polarization characteristics.
Outdoor channel measurements				
[47]	141-148.5	VNA with RoF	Double directional	PL, AS, and cluster spread.

In UWB communication systems at sub-THz bands, high-speed ADCs are the core devices which affect system performance. However, the requirements for high speed and high resolution increase the system cost [115]. Generally speaking, there are two methods to achieve a high-speed ADC. The first one is the SiGe BiCMOS ADC, which has a high device cut-off frequency and can support the circuit to operate at a high frequency [116]. However, this ADC requires great power consumption and is at a low-resolution, as demonstrated in [117]. The other one is the multiple time-interleaved ADC. Due to the rapid development of the CMOS technologies, the high intergration and low power consumption can be realized in this ADC circuit [118]. However, it faces some problems such as the complexity of the multiple interleaved channels and corresponding calibration circuits [116]. Recent work reported in [118]–[120] demonstrated that the sampling rate of the high-speed ADCs can be achieved to dozens of GS/s.

B. Review on sub-THz channel measurements

For the propagation mechanism of different materials at the sub-THz bands, the THz-TDS is mainly used for this purpose in the literature. The reflection properties of two stratified building materials, i.e., a double pane window and white paint on plaster, at different angles in the frequency range from 100 to 500 GHz were measured and investigated by THz-TDS in [89]. Besides, a ray tracing (RT) simulation for a sample indoor scenario at 350 GHz was presented. The simulation results agreed well with the measured reflection coefficients. The absorption and reflection properties at different angles from 100 to 350 GHz of three typical building materials, i.e., plaster, wood, and glass, were measured using THz-TDS and presented in [101]. The reflection coefficients were also calculated using Fresnel's equations. The measurement results and the calculated values were in a good agreement, which demonstrated that the THz-TDS can be used as an efficient tool to characterize reflection properties of diverse materials. The angle- and frequency-dependent measurements from 0.1 to 1 THz using THz-TDS and the reflection model of materials with a rough surface based on the Kirchhoff scattering theory were presented in [102]. Furthermore, a RT algorithm with an advanced Kirchhoff model considering randomly rough, normally distributed surfaces was proposed and used to simulate the signal coverage of a typical office scenario. It showed that with a low surface roughness, a high data rate of 20 Gbit/s can be reached, while under a high roughness condition, the communication would be failed. The propagation mechanism can also be investigated by using VNA-based sounder and correlation-based sounder. Channel measurements at 140 GHz were conducted using correlation-based sounder in [19] to investigate the surface roughness influence on scattering behavior between the mm-wave and sub-THz bands, and to validate the Directive Scattering theory.

For the channel characteristics, many efforts on large-scale channel characteristics, i.e., pathloss and shadowing measurements, and delay dispersion analysis and modeling using VNA based sounder or correlation-based sounder at sub-THz bands in various indoor and outdoor scenarios, such as 140 GHz and 300 GHz bands, were made in [8], [59]–[61], [70], [103]. Those PL model illustrated a large PL at sub-THz bands compared to that at the lower frequency bands. Those models provided basic large-scale characteristics of the sub-THz channel and made contributions to the future channel measurements and analysis. In [104] and [121], the channel measurements in the train scenario were conducted by the correlation-based channel sounder in [53] and the large-scale characteristics, K-factor and DS were presented. In addition, measurement-validated RT simulation methods were proposed and utilized to simulate train station channel model and intra-wagon channel model for future B5G system design, deployment, and evaluation.

For the directional channel characteristics, a VNA based double directional channel measurements at sub-THz bands were conducted in [69]. K-factors, DSs and angular spreads (ASs) were presented. In addition, a virtual 2×2 MIMO measurementwas conducted in this paper. A measurement-validated frequency domain RT method was presented and demonstrated to be well-suited to simulate the sub-THz indoor channel. Double directional outdoor measurements across the frequency bands from 141 to 148.5 GHz using VNA based channel sounder with RoF techniques were conducted in [47]. The results showed large ASs of the angle of arrival (AoA) and angle of departure (AoD). In [33], VNA based directional channel measurements at 28 and 140 GHz in a shopping mall scenario were conducted. The DS and AS of 28 and 140 GHz were found to be similar. After using a cluster-based algorithm to estimate multipath components (MPCs), the results illustrated that the number of MPCs is smaller at 140 GHz than that at 28 GHz. Indoor double directional channel measurements using correlation-based channel sounder at the frequency bands of 10, 60 GHz and 300 GHz were conducted in [97]. The results showed that the multipath richness of the radio channel was frequency-dependent, and the multipath richness at 300 GHz decreased compared to that of 60 GHz. For the channel characteristics in dynamic scenarios, the correlation-based channel sounder is suitable for obtaining the Doppler shift at sub-THz bands. However, to our knowledge, no literature has investigated this yet.

Some measurements and analysis of sub-THz MIMO channel based on VNA were presented in [52], [122]. In [52], PL, shadowing, DS and Doppler shift of a 4×4 MIMO in a data center scenario were presented. The throughput analysis of 2×2 MIMO across the frequency spectrum from 298 to 313 GHz in comparison with the single-input-single-output (SISO) channel was presented in [122]. The results showed that MIMO can significantly increase the throughput from 5.5 Gb/s to 7 Gb/s.

V. A VNA BASED CHANNEL SOUNDING SYSTEM

In this section, a VNA based channel sounder operating from 220 to 330 GHz is introduced, and the performance of this sounder are presented and evaluated.

A. Sounder architecture

The type of VNA and the frequency extender used in the sub-THz channel sounder are Keysight N5227B [123] and VDI WR3.4 [51], respectively. Fig. 4 (a) and Table IV illustrate the schematic diagram and configurations of the devices, respectively. As shown in Fig. 4 (a), at the Tx side, signals from 12.222 to 18.333 GHz are sent from port 1 resulting in sub-THz signals from 220 to 330 GHz after passing through an 18 times multiplier. The signals are divided into two signals by a coupler, one of which is used to transmit through a horn antenna with 25 dBi antenna gain and 8 half power beamwidth (HPBW) [124] and the other is used to generate 100 MHz reference signals. Note that port 3 sends LO signals from 9.162 to 13.746 GHz. The LO signals are split by a signal splitter and multiplied to the frequency range from 219.9 to 329.9 GHz

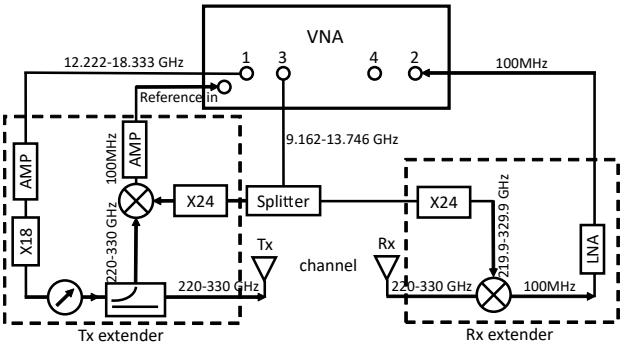

(a)

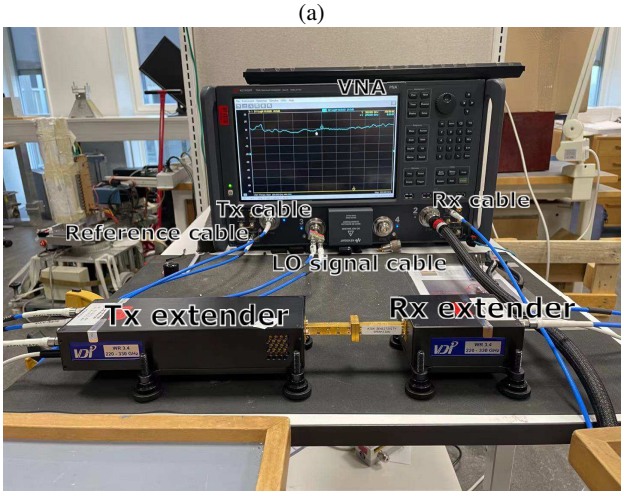

(b)

Fig. 4: The photos of the VNA based channel sounder at sub-THz bands. (a) The schematic diagram; (b) The photo of the link budget measurement setup.

TABLE IV: The configuration of the sub-THz sounder.

Parameter	Value
VNA type	N5227B
Extender type	WR3.4
Start frequency (GHz)	220
End frequency (GHz)	330
Frequency point	11001
VNA Transmitted power (dBm)	9
Antenna type	Horn
Antenna gain (dBi)	25
HPBW (deg)	8

by 24 times multiplier. At the Rx side, the received signal is demodulated to 100 MHz, amplified by an LNA and sent to port 2. The S_{21} parameter can be obtained from the result of dividing the 100 MHz received signal by the reference signal.

B. Link budget analysis

Fig. 4 (b) depicts the link budget measurement setup. At the Tx and the Rx side, 5-meter RF cables were used to connect the VNA with the extenders. Fig. 5 illustrates the link budget of the channel sounder at 275 GHz. In order to ensure that the Tx extender works normally and prevent damage, the transmitted power from port 1 is 9 dBm. The gains of the Tx extender and Rx extender are 2.6 and 15.3 dB, respectively. Compared to 8.8 dB RF cable loss (12.22-18.33 GHz) at the Tx side, thanks to the 100 MHz received

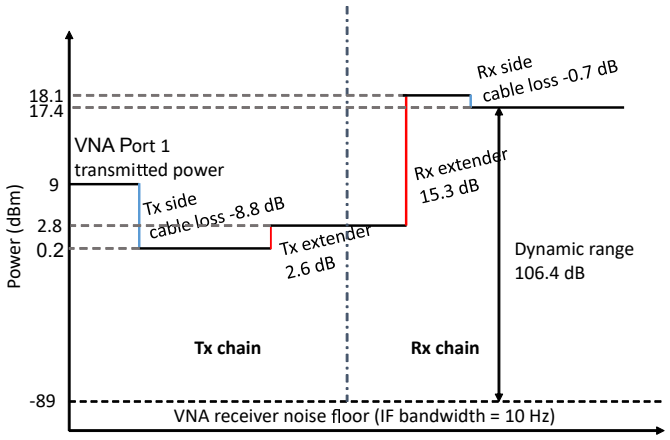

Fig. 5: The link budget of the VNA based channel sounder at 275 GHz.

signal, the RF cable loss is extremely low at Rx side. The dynamic range is 106.4 dB at the IF bandwidth of 10 Hz, which can support for the channel measurements at distances below 10 meters (cable limitation). The measurement range can be increased by lengthening the RF cable length at the Rx side. In our future work, we plan to apply RoF techniques at the Tx side to achieve long distance measurements and to apply the phase-compensated method in [62] for the phase measurements at sub-THz bands.

C. System stability over long measurement time

During the entire measurement period, it is crucial that the channel sounder is stable. Generally speaking, spatial domain measurements can span several hours to record channel response data. To verify the robustness of this system, a back-to-back measurement in the same scenario as the link budget scenario in Fig. 4 (b) was conducted within 13 hours with 1-minute interval resulting in 780 snapshots. Other measurement configurations are the same as those in Table IV. The amplitude and phase stability of the system response are illustrated in Fig 6. The amplitude results are displayed in decibel scale. The power varies from $[13.3, 13.4]$ dB, $[9.9, 10.0]$ dB, $[12.8, 12.9]$ dB at 220 GHz, 275 GHz, and 330 GHz, respectively, while the phase varies in the range of $[-66.2°, -58.0°]$, $[13.5°, 18.7°]$, $[-102.9°, -97.2°]$ at 220 GHz, 275 GHz, and 330 GHz, respectively. The power drops from 17.5 to 6.5 dB in the frequency range of 228-251 GHz and increases from 7.7 to 12.9 dB in the frequency range from 267 to 330 GHz, as shown in Fig. 6 (c), possibly due to the working performance of the frequency mixer at these bands. Note that the system response is calibrated before the measurements, thus, it will not affect the measurement results. Overall, the amplitude and phase of this system were observed to be stable, as shown in Fig. 6.

D. Calibration investigation

Calibration is also an essential part for channel measurements. Before the channel measurement, a normalization procedure is usually carried out to deembed the system response

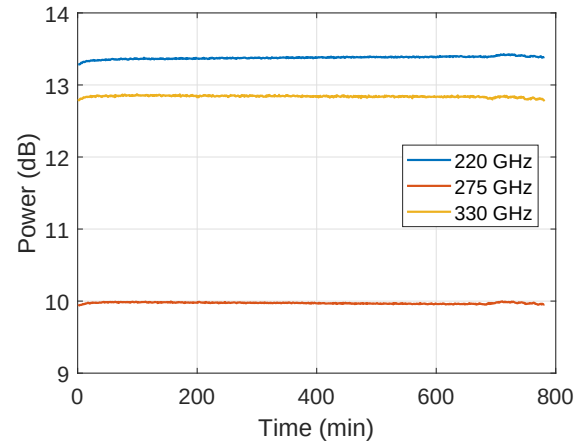

(a)

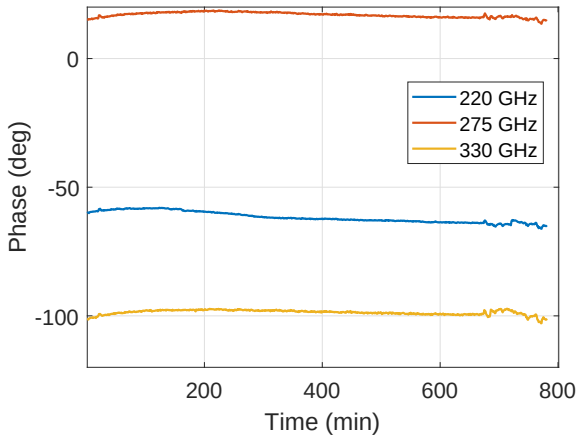

(b)

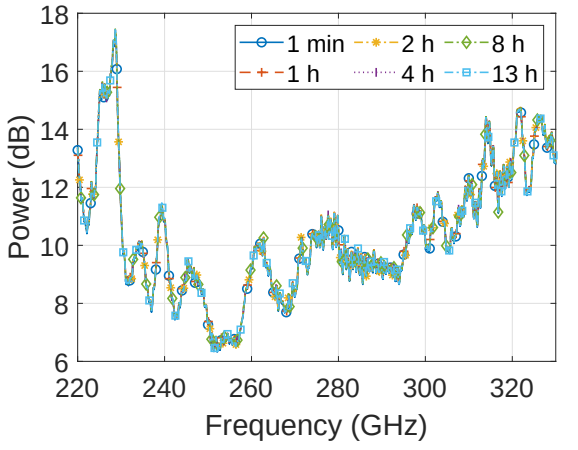

(c)

Fig. 6: The results of the stability measurements. (a) The amplitude stability; (b) The phase stability; (c) System response of the channel sounder in the back-to-back measurements over a period of 13 hours.

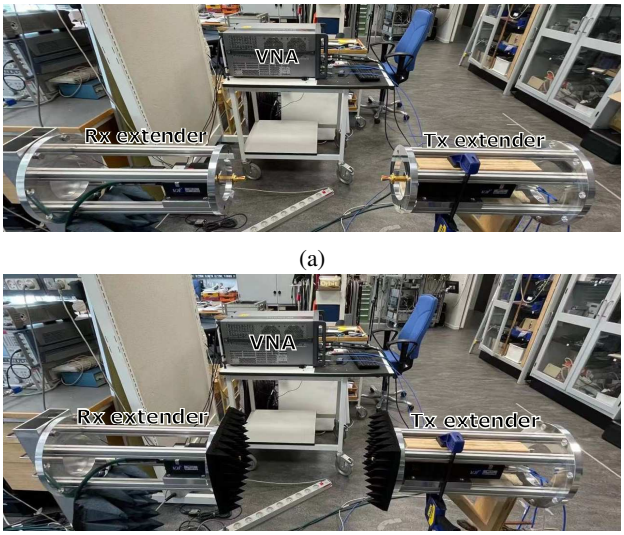

Fig. 7: The photos of the channel measurement setup. (a) The photo of the channel measurement setup without absorber;(b) The photo of the channel measurement setup with absorber.

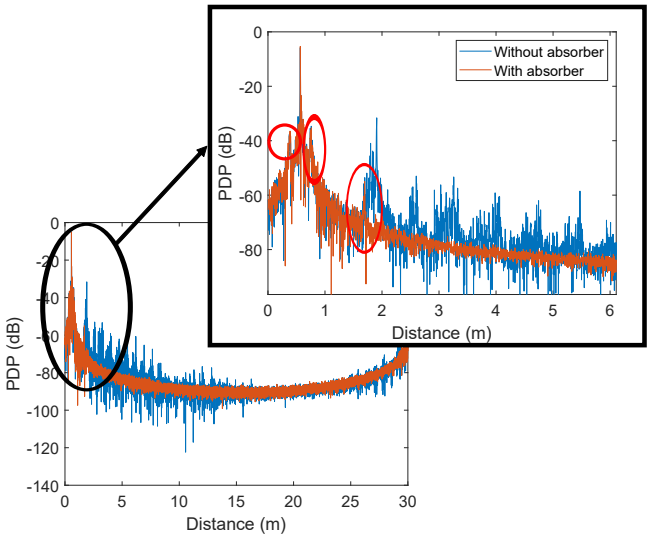

Fig. 8: The comparison of the PDPs with and without absorbers at the distance of 0.4 m.

in the back-to-back measurement shown in Fig.4 (b). The measurement is to verify the efficiency of absorbers placed around the antennas. Firstly, a back-to-back measurement and a normalization procedure were conducted to calibrate the system response. Then the comparison channel measurements with and without absorbers at the distance of 0.4 m were conducted, as shown in Fig. 7. As demonstrated in Fig. 8 of the comparison of the power delay profiles (PDPs), the use of the absorbers can significantly eliminate the spurious peaks. However, some unexpected spurious peaks still appeared in the red area, possibly due to the non-ideal absorbers for sub-THz bands.

TABLE V: The configuration of the double directional channel measurements.

Parameter	Value
Frequency range (GHz)	$250-300$
Bandwidth	50
Frequency point	15001
Tx-Rx distance (m)	2.25
Antenna height (m)	0.9
Tx azimuth range (deg)	$[-90, 90]$
Tx rotating step (deg)	6
Rx azimuth range (deg)	$[-180, 179]$
Rx rotating step (deg)	6

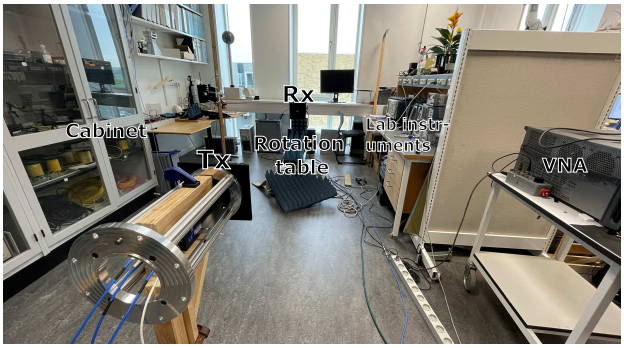

Fig. 9: Picture of the laboratory scenario.

E. Directional measurements and results

1) Scenario description: Double directional measurements were conducted in a laboratory scenario with rich scatterers, e.g., cabinet and lab instruments, as shown in Fig. 9. Note that a back-to-back calibration is performed before the measurements. During these measurements, a double directional measurement scheme is employed with two identical 8° HPBW horn antennas, both for both Tx and Rx sides. The boresight of the Rx is set to rotate in azimuth within the range of $[-180^\circ, 179^\circ]$ in step of 6°, which results in 60 steps in azimuth. The Tx antenna is fixed while the Rx is rotated. After the rotation of the Rx, the Tx is rotated within the range of $[-90^\circ, 90^\circ]$ in step of 6°. Thus, we can obtain $31 \times 60 = 1860$ channel responses in total. Table V illustrates the configuration in the directional channel measurements.

2) Signal model: In this study, the static CIR can be written as:

$$h(\tau) = \sum_{\ell=1}^{L} \alpha_\ell \delta\left(\tau - \tau_\ell\right) \delta\left(\Omega - \Omega_{DoD,\ell}\right) \delta\left(\Omega - \Omega_{DoA,\ell}\right), \tag{7}$$

where α_ℓ, τ_ℓ, $\Omega_{DoD,\ell}$, and $\Omega_{DoA,\ell}$ represent the complex attenuation, the delay, the direction-of-departure (DoD) set, the direction-of-arrival (DoA) set of the ℓth MPC, respectively. L denotes the total number of propagation paths.

3) Measurement results: Fig. 10 illustrates the power angular delay profile (PADP) at the AoD of 0 degree and the power angle spectrum from the raw measured data. The distance of the line-of-sight (LoS) path (i.e. 2.25 m), which corresponding to 7.5 ns in the PADP, as shown in Fig. 10 (a). Besides, weak reflections from the crossbar and wall are detected in the opposite direction of the LoS and the delay of 18.5 and 23

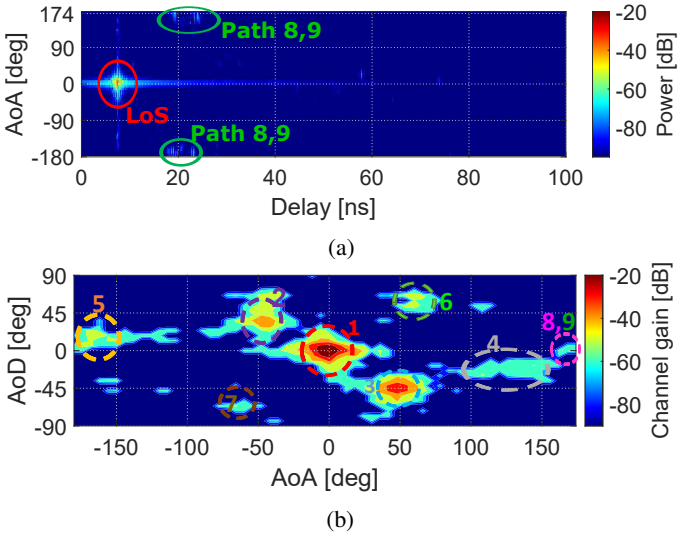

Fig. 10: Double directional measurement results in the lab scenario. (a) The example PADP at the AoD of 0 degree; (b) Power angle spectrum.

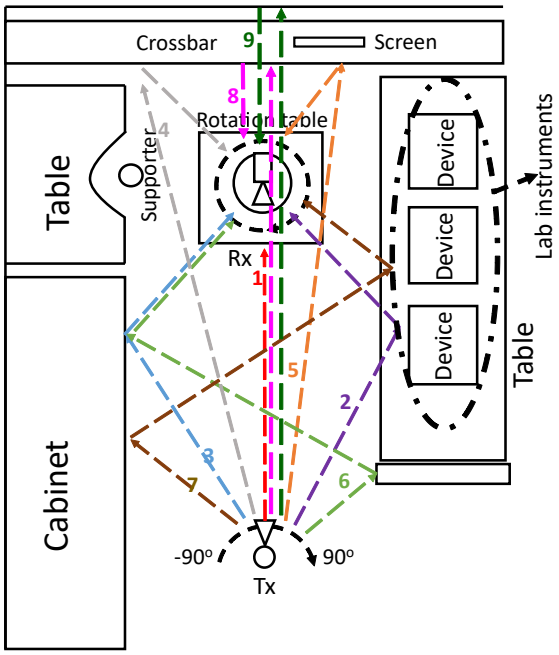

Fig. 11: Relation of the main MPCs to the scenario.

ns, respectively. The channel gain demonstrated in Fig. 10 (b) is calculated as the sum of the power 3-dB above the noise floor at a specific AoA and AoD. The relationship between the identified multipath components (MPCs) and the scenario is depicted in Fig. 11. Comparing Fig. 10 (b) and Fig. 11, the AoAs and AoDs of the main MPCs are found to be well-matched with the scenario. Furthermore, the link distances of the main MPCs in the PDP are also calculated, and it is observed that they match the scenario well.

VI. Sub-THz challenge and Future works

Although many efforts have been given for the sub-THz channel sounding techniques, measurements and modeling, we still face many challenges:

- As shown in the Section III, the current channel sounding techniques have their drawbacks, e.g., the channel sounder with the SG and SA is only capable for power-based measurements, the sweep time of the VNA-based channel sounder is generally long and the sounder is only suitable for static scenario, the correlation-based channel sounder has much smaller bandwidth compared to VNA-based channel sounder and THz-TDS, and the dynamic range of the THz-TDS is low and the size of the spectrometer is large. Besides, the measurement capability at sub-THz bands is still far from what it was at sub-6 GHz, e.g., Prosound channel sounder [125]. Moreover, reconfigurable intelligent surface (RIS) is a hot topic in Beyond 5G research. However, the channel sounders for RIS measurements are still in their infancy and channel sounders are needed to support RIS research. To sum up, new technologies need to be applied to improve the channel sounder.
- There has been no standard sub-THz channel model so far. Measurements are needed to reach the conclusion whether the existing channel model at mm-wave bands, such as 3GPP FR2 models, can be extended to sub-THz bands. Moreover, the standardized channel model below 100 GHz generally separates the propagation channels and antennas. However, antennas with high gain and narrow beamwidth will be applied for the sub-THz channel measurements and it is unclear whether it is necessary to deembed the antenna response and estimate the propagation parameters.
- Although sub-THz channels have been measured in some short distance and indoor scenarios, as illustrated in Table III, channel sounding and modeling for different frequency bands and different application scenarios, e.g. large hall and train-to-infrastructure, are not sufficient now. Besides, the MIMO techniques should be taken into account and the MIMO channel at sub-THz bands needs to be studied.
- Simulation-based channel modeling is also crucial for sub-THz bands since channel measurements are always costly and subject to uncertainties, and limited to certain scenarios due to the size and capability of the channel sounder, e.g., the current size and weight of sub-THz channel sounder is impractical for unmanned aircraft vehicle (UAV) channel measurements. RT has become a popular simulation tool for sub-THz channel modeling, e.g., in [69], [126]. Channel measurements are required to obtain the material parameters and to calibrate and validate the RT simulation. However, most of the ray-tracing tools currently provide modeling up to GHz frequencies only [127] and the existing ray-tracing tools are not sufficient for sub-THz bands. Hence, sub-THz simulation tools are required to be developed for channel modeling at sub-THz bands.
- New features at sub-THz bands, e.g., ultrawide band, have motivated new applications enabled by sub-THz channel modeling and sensing. Medical and security applications

based on sub-THz and THz bands have been developed [128]. However, these sub-THz applications and productions face many challenges such as power-efficient devices and cost-effective integrated circuit [19]. Other potential applications at sub-THz bands have been discussed in [3], [19], [96], e.g., centimeter-level positioning and THz imaging. However, these potential applications are still under investigation.

So far, design of sub-THz channel sounding techniques and research on measurements and modeling are still in their infancy, and further efforts are needed to support the design and deployment of future sub-THz communication systems.

VII. Conclusions

This paper has provided a deep look into the requirements, approaches, reviews and future challenge of channel sounding techniques at sub-THz bands. This paper first introduced the recent recommendations and standard activities of countries and organizations to promote the development of future wireless communication systems at sub-THz frequency bands. The requirements of an ideal sounder and the uniqueness of the channel sounders at sub-THz bands were described in this paper. Besides, based on these requirements, the main types of channel sounding techniques were presented and compared. The state-of-the-art sub-THz channel sounders and channel measurements in terms of these sounding techniques were presented. A VNA-based channel sounder across the frequency bands from 220 to 330 GHz was then presented, and the performance of this channel sounder was evaluated. Double directional measurements using this VNA-based channel sounder from 250 to 300 GHz was conducted, the measurement results showed that the main MPCs matched the scenario well. Furthermore, based on the infancy of the existing sounding techniques, measurements and modeling at sub-THz bands, the sub-THz challenge and future outlook were presented.

References

[1] K. Rikkinen, P. Kyösti, M. E. Leinonen, M. Berg, and A. Parssinen, "THz radio communication: Link budget analysis toward 6G," *IEEE Communications Magazine*, vol. 58, no. 11, pp. 22–27, 2020.

[2] T. Kürner, "Turning THz communications into reality: Status on technology, standardization and regulation," in *2018 43rd International Conference on Infrared, Millimeter, and Terahertz Waves (IRMMW-THz)*, 2018, pp. 1–3.

[3] A. Pärssinen, M.-S. Alouini, M. Berg, T. Kürner, P. Kyösti, M. E. Leinonen, M. Matinmikko-Blue, E. McCune, U. Pfeiffer, and P. Wambacq, "White paper on RF enabling 6G opportunities and challenges from technology to spectrum," *6G Flagship Ecosystem*, Apr. 2021. [Online]. Available: https://www.6gchannel.com/items/6g-white-paper-rf-spectrum/

[4] ITU-R, "Attenuation by atmospheric gases," *Recommendation P.676-10*, 2013.

[5] J. Ma, R. Shrestha, L. Moeller, and D. M. Mittleman, "Invited article: Channel performance for indoor and outdoor terahertz wireless links," *APL Photonics*, vol. 3, no. 5, p. 051601, 2018. [Online]. Available: https://doi.org/10.1063/1.5014037

[6] T. Schneider, A. Wiatrek, S. Preussler, M. Grigat, and R. Braun, "Link budget analysis for terahertz fixed wireless links," *IEEE Transactions on Terahertz Science and Technology*, vol. 2, no. 2, pp. 250–256, 2012.

[7] M. Marcus and B. Pattan, "Millimeter wave propagation: spectrum management implications," *IEEE Microwave Magazine*, vol. 6, no. 2, pp. 54–62, 2005.

[8] Y. Xing and T. S. Rappaport, "Propagation measurement system and approach at 140 GHz-moving to 6G and above 100 GHz," in *2018 IEEE Global Communications Conference (GLOBECOM)*, 2018, pp. 1–6.

[9] ESTI, "Millimeter wave transmission (mWT); applications and use casesof millimeter wave transmission," Sophia Antipolis, France, Aug. 2015.

[10] "IEEE standard for high data rate wireless multi-media networks–amendment 2: 100 Gb/s wireless switched point-to-point physical layer," *IEEE Std 802.15.3d-2017 (Amendment to IEEE Std 802.15.3-2016 as amended by IEEE Std 802.15.3e-2017)*, pp. 1–55, 2017.

[11] FCC, "FCC opens spectrum horizons for new services and technologies," Mar. 2019. [Online]. Available: https://www.fcc.gov/document/fcc-opens-spectrum-horizons-new-services-technologies

[12] M. J. Marcus, "WRC-19 issues: Agenda item 1.15 and the use of 275 - 450 GHz," *IEEE Wireless Communications*, vol. 23, no. 6, pp. 2–3, 2016.

[13] A. Molisch, *Wireless communications*. John Wiley & Sons Ltd., 2011.

[14] C. Gentile, A. F. Molisch, J. Chuang, D. G. Michelson, A. Bodi, A. Bhardwaj, O. Ozdemir, W. A. G. Khawaja, I. Guvenc, Z. Cheng, F. Rottenberg, T. Choi, R. Mller, N. Han, and D. Dupleich, "Methodology for benchmarking radio-frequency channel sounders through a system model," *IEEE Transactions on Wireless Communications*, vol. 19, no. 10, pp. 6504–6519, 2020.

[15] Z. Ma, B. Ai, R. He, G. Wang, Y. Niu, and Z. Zhong, "A wideband non-stationary air-to-air channel model for uav communications," *IEEE Transactions on Vehicular Technology*, vol. 69, no. 2, pp. 1214–1226, 2020.

[16] Z. Ma, B. Ai, R. He, G. Wang, Y. Niu, M. Yang, J. Wang, Y. Li, and Z. Zhong, "Impact of uav rotation on mimo channel characterization for air-to-ground communication systems," *IEEE Transactions on Vehicular Technology*, vol. 69, no. 11, pp. 12 418–12 431, 2020.

[17] Z. Ma, B. Ai, R. He, Z. Zhong, and M. Yang, "A non-stationary geometry-based mimo channel model for millimeter-wave uav networks," *IEEE Journal on Selected Areas in Communications*, vol. 39, no. 10, pp. 2960–2974, 2021.

[18] X. Yin and X. Cheng, *Propagation Channel Characterization, Parameter Estimation and Modeling for Wireless Communications*. John Wiley & Sons, IEEE, 2016.

[19] T. S. Rappaport, Y. Xing, O. Kanhere, S. Ju, A. Madanayake, S. Mandal, A. Alkhateeb, and G. C. Trichopoulos, "Wireless communications and applications above 100 GHz: Opportunities and challenges for 6G and beyond," *IEEE Access*, vol. 7, pp. 78 729–78 757, 2019.

[20] J.-h. Zhang, P. Tang, L. Yu, T. Jiang, and L. Tian, "Channel measurements and models for 6G: current status and future outlook," *Frontiers of information technology & electronic engineering*, vol. 21, no. 1, pp. 39–61, 2020.

[21] T. S. Rappaport, "Characterization of UHF multipath radio channels in factory buildings," *IEEE Transactions on Antennas and Propagation*, vol. 37, no. 8, pp. 1058–1069, 1989.

[22] D. A. Hawbaker and T. S. Rappaport, "Indoor wideband radio propagation measurement system at 1.3 GHz and 4.0 GHz," in *40th IEEE Conference on Vehicular Technology*, 1990, pp. 626–630.

[23] T. Zwick, T. J. Beukema, and Haewoon Nam, "Wideband channel sounder with measurements and model for the 60 GHz indoor radio channel," *IEEE Transactions on Vehicular Technology*, vol. 54, no. 4, pp. 1266–1277, 2005.

[24] P. Truffer and P. E. Leuthold, "Wide-band channel sounding at 24 GHz based on a novel fiber-optic synchronization concept," *IEEE Transactions on Microwave Theory and Techniques*, vol. 49, no. 4, pp. 692–700, 2001.

[25] M. Lei, J. Zhang, T. Lei, and D. Du, "28-GHz indoor channel measurements and analysis of propagation characteristics," in *2014 IEEE 25th Annual International Symposium on Personal, Indoor, and Mobile Radio Communication (PIMRC)*, 2014, pp. 208–212.

[26] Y. Rissafi, L. Talbi, and M. Ghaddar, "Experimental characterization of an UWB propagation channel in underground mines," *IEEE Transactions on Antennas and Propagation*, vol. 60, no. 1, pp. 240–246, 2012.

[27] Y. Lv, X. Yin, C. Zhang, and H. Wang, "Measurement-based characterization of 39 GHz millimeter-wave dual-polarized channel under foliage loss impact," *IEEE Access*, vol. 7, pp. 151 558–151 568, 2019.

[28] G. R. MacCartney and T. S. Rappaport, "A flexible millimeter-wave channel sounder with absolute timing," *IEEE Journal on Selected Areas in Communications*, vol. 35, no. 6, pp. 1402–1418, 2017.

[29] J. Hejselbaek, Y. Ji, W. Fan, and G. F. Pedersen, "Channel sounding system for mm-wave bands and characterization of indoor propagation

at 28 GHz," *International journal of wireless information networks*, vol. 24, no. 3, pp. 204–216, 2017.

[30] D. Cassioli, M. Z. Win, and A. F. Molisch, "The ultra-wide bandwidth indoor channel: from statistical model to simulations," *IEEE Journal on Selected Areas in Communications*, vol. 20, no. 6, pp. 1247–1257, 2002.

[31] P. Bello, "Characterization of randomly time-variant linear channels," *IEEE Transactions on Communications Systems*, vol. 11, no. 4, pp. 360–393, 1963.

[32] J. O. Nielsen, W. Fan, P. C. F. Eggers, and G. F. Pedersen, "A channel sounder for massive MIMO and mmwave channels," *IEEE Communications Magazine*, vol. 56, no. 12, pp. 67–73, 2018.

[33] S. L. H. Nguyen, J. Jrvelinen, A. Karttunen, K. Haneda, and J. Putkonen, "Comparing radio propagation channels between 28 and 140 GHz bands in a shopping mall," in *12th European Conference on Antennas and Propagation (EuCAP 2018)*, 2018, pp. 1–5.

[34] Q. Zhu, H. Li, Y. Fu, C.-X. Wang, Y. Tan, X. Chen, and Q. Wu, "A novel 3d non-stationary wireless mimo channel simulator and hardware emulator," *IEEE Transactions on Communications*, vol. 66, no. 9, pp. 3865–3878, 2018.

[35] Q. Zhu, Y. Yang, C.-X. Wang, Y. Tan, J. Sun, X. Chen, and W. Zhong, "Spatial correlations of a 3-d non-stationary mimo channel model with 3-d antenna arrays and 3-d arbitrary trajectories," *IEEE Wireless Communications Letters*, vol. 8, no. 2, pp. 512–515, 2019.

[36] W. Fan, I. Carton, J. . Nielsen, K. Olesen, and G. F. Pedersen, "Measured wideband characteristics of indoor channels at centimetric and millimetric bands," *EURASIP journal on wireless communications and networking*, vol. 2016, no. 1, pp. 1–13, 2016.

[37] A. W. Mbugua, W. Fan, Y. Ji, and G. F. Pedersen, "Millimeter wave multi-user performance evaluation based on measured channels with virtual antenna array channel sounder," *IEEE Access*, vol. 6, pp. 12 318–12 326, 2018.

[38] J. Salmi and A. F. Molisch, "Propagation parameter estimation, modeling and measurements for ultrawideband MIMO radar," *IEEE Transactions on Antennas and Propagation*, vol. 59, no. 11, pp. 4257–4267, 2011.

[39] T. 38.827, "Study on radiated metrics and test methodology for the verification of multi-antenna reception performance of NR user equipment (UE),," V1.3.1, Tech. Rep., 2020.

[40] J. Zhang, Y. Zhang, Y. Yu, R. Xu, Q. Zheng, and P. Zhang, "3-D MIMO: How much does it meet our expectations observed from channel measurements?" *IEEE Journal on Selected Areas in Communications*, vol. 35, no. 8, pp. 1887–1903, 2017.

[41] X. Gao, O. Edfors, F. Rusek, and F. Tufvesson, "Massive MIMO performance evaluation based on measured propagation data," *IEEE Transactions on Wireless Communications*, vol. 14, no. 7, pp. 3899–3911, 2015.

[42] J. Hejselbk, J. . Nielsen, W. Fan, and G. F. Pedersen, "Measured 21.5 GHz indoor channels with user-held handset antenna array," *IEEE Transactions on Antennas and Propagation*, vol. 65, no. 12, pp. 6574–6583, 2017.

[43] P. B. Papazian, C. Gentile, K. A. Remley, J. Senic, and N. Golmie, "A radio channel sounder for mobile millimeter-wave communications: System implementation and measurement assessment," *IEEE Transactions on Microwave Theory and Techniques*, vol. 64, no. 9, pp. 2924–2932, 2016.

[44] Z. Ying, K. Zhao, E. Bengtsson, H. Tataria, and F. Tufvesson, "Design of switched antenna arrays for a 28 GHz propagation channel sounder," in *2020 IEEE International Symposium on Antennas and Propagation and North American Radio Science Meeting*, 2020, pp. 55–56.

[45] M. Kyr, S. Ranvier, V. Kolmonen, K. Haneda, and P. Vainikainen, "Long range wideband channel measurements at 8186 ghz frequency range," in *Proceedings of the Fourth European Conference on Antennas and Propagation*, 2010, pp. 1–5.

[46] K. Yang, T. Roste, F. Bekkadal, K. Husby, and O. Trandem, "Long-distance propagation measurements of mobile radio channel over sea at 2 ghz," in *2011 IEEE Vehicular Technology Conference (VTC Fall)*, 2011, pp. 1–5.

[47] N. A. Abbasi, A. Hariharan, A. M. Nair, A. S. Almaiman, F. B. Rottenberg, A. E. Willner, and A. F. Molisch, "Double directional channel measurements for THz communications in an urban environment," in *ICC 2020 - 2020 IEEE International Conference on Communications (ICC)*, 2020, pp. 1–6.

[48] S. Ranvier, M. Kyro, K. Haneda, T. Mustonen, C. Icheln, and P. Vainikainen, "VNA-based wideband 60 GHz MIMO channel sounder with 3-D arrays," in *2009 IEEE Radio and Wireless Symposium*, 2009, pp. 308–311.

[49] X. Cai, G. Zhang, C. Zhang, W. Fan, J. Li, and G. F. Pedersen, "Dynamic channel modeling for indoor millimeter-wave propagation channels based on measurements," *IEEE Transactions on Communications*, vol. 68, no. 9, pp. 5878–5891, 2020.

[50] J. V. Rudd, D. A. Zimdars, and M. W. Warmuth, "Compact fiber-pigtailed terahertz imaging system," in *Commercial and Biomedical Applications of Ultrafast Lasers II*, J. Neev and M. K. Reed, Eds., vol. 3934, International Society for Optics and Photonics. SPIE, 2000, pp. 27 – 35.

[51] V. WR3.4. [Online]. Available: https://www.vadiodes.com/en/wr3-4vnax

[52] C. Cheng, S. Sangodoyin, and A. Zaji, "Terahertz MIMO fading analysis and Doppler modeling in a data center environment," in *2020 14th European Conference on Antennas and Propagation (EuCAP)*, 2020, pp. 1–5.

[53] S. Rey, J. M. Eckhardt, B. Peng, K. Guan, and T. Krner, "Channel sounding techniques for applications in THz communications: A first correlation based channel sounder for ultra-wideband dynamic channel measurements at 300 GHz," in *2017 9th International Congress on Ultra Modern Telecommunications and Control Systems and Workshops (ICUMT)*, 2017, pp. 449–453.

[54] P. Kyösti, K. Haneda, J.-M. Conrat, and A. Pärssinen, "Above-100 GHz wave propagation studies in the european project Hexa-X for 6G channel modelling," in *2021 Joint European Conference on Networks and Communications 6G Summit (EuCNC/6G Summit)*, 2021, pp. 538–543.

[55] J. Hejselbk, J. . Nielsen, C. Drewes, W. Fan, and G. F. Pedersen, "Propagation measurements for device-to-device communication in forest terrain," in *12th European Conference on Antennas and Propagation (EuCAP 2018)*, 2018, pp. 1–5.

[56] J. Neu and C. A. Schmuttenmaer, "Tutorial: An introduction to terahertz time domain spectroscopy (THz-TDS)," *Journal of Applied Physics*, vol. 124, no. 23, p. 231101, 2018.

[57] P. Bawuah, D. Markl, D. Farrell, M. Evans, A. Portieri, A. Anderson, D. Goodwin, R. Lucas, and J. A. Zeitler, "Terahertz-based porosity measurement of pharmaceutical tablets: a tutorial," *Journal of infrared, millimeter and terahertz waves*, vol. 41, no. 4, pp. 450–469, 2020.

[58] H. Harde, R. A. Cheville, and D. Grischkowsky, "Terahertz studies of collision-broadened rotational lines," *The Journal of Physical Chemistry A*, vol. 101, no. 20, pp. 3646–3660, 1997. [Online]. Available: https://doi.org/10.1021/jp962974c

[59] S. Priebe, C. Jastrow, M. Jacob, T. Kleine-Ostmann, T. Schrader, and T. Krner, "Channel and propagation measurements at 300 GHz," *IEEE Transactions on Antennas and Propagation*, vol. 59, no. 5, pp. 1688–1698, May 2011.

[60] Y. Zantah, M. Alissa, T. Kreul, and T. Kaiser, "Ultra-wideband multipath channel characterization at 300 GHz," in *WSA 2020; 24th International ITG Workshop on Smart Antennas*, 2020, pp. 1–5.

[61] S. Kim, W. T. Khan, A. Zaji, and J. Papapolymerou, "D-band channel measurements and characterization for indoor applications," *IEEE Transactions on Antennas and Propagation*, vol. 63, no. 7, pp. 3198–3207, 2015.

[62] A. W. Mbugua, W. Fan, K. Olesen, X. Cai, and G. F. Pedersen, "Phase-compensated optical fiber-based ultrawideband channel sounder," *IEEE Transactions on Microwave Theory and Techniques*, vol. 68, no. 2, pp. 636–647, 2020.

[63] J. Huang, C. Wang, R. Feng, J. Sun, W. Zhang, and Y. Yang, "Multi-frequency mmwave massive MIMO channel measurements and characterization for 5G wireless communication systems," *IEEE Journal on Selected Areas in Communications*, vol. 35, no. 7, pp. 1591–1605, 2017.

[64] D. K. Ghodgaonkar, V. V. Varadan, and V. K. Varadan, "A free-space method for measurement of dielectric constants and loss tangents at microwave frequencies," *IEEE Transactions on Instrumentation and Measurement*, vol. 38, no. 3, pp. 789–793, June 1989.

[65] T. Dammes, W. Endemann, and R. Kays, "Frequency domain channel measurements for wireless localization - practical considerations and effects of the measurement," in *European Wireless 2012; 18th European Wireless Conference 2012*, 2012, pp. 1–8.

[66] G. Zhang, J. . Nielsen, X. Cai, K. Saito, P. Hanpinitsak, J. I. Takada, G. F. Pedersen, and W. Fan, "Modeling multi-frequency characteristics for classroom and hall scenarios at 2-4, 9-11 and 27-29 GHz bands," *IEEE Access*, vol. 9, pp. 14 549–14 563, 2021.

[67] J. Jrvelinen, K. Haneda, and A. Karttunen, "Indoor propagation channel simulations at 60 GHz using point cloud data," *IEEE Transactions on Antennas and Propagation*, vol. 64, no. 10, pp. 4457–4467, 2016.

[68] N. Khalid and O. B. Akan, "Wideband THz communication channel measurements for 5G indoor wireless networks," in *2016 IEEE International Conference on Communications (ICC)*, 2016, pp. 1–6.

[69] S. Priebe, M. Kannicht, M. Jacob, and T. Krner, "Ultra broadband indoor channel measurements and calibrated ray tracing propagation modeling at THz frequencies," *Journal of Communications and Networks*, vol. 15, no. 6, pp. 547–558, 2013.

[70] L. Pometcu and R. DErrico, "An indoor channel model for high data-rate communications in D-band," *IEEE Access*, vol. 8, pp. 9420–9433, 2020.

[71] N. A. Abbasi, A. Hariharan, A. M. Nair, and A. F. Molisch, "Channel measurements and path loss modeling for indoor THz communication," in *2020 14th European Conference on Antennas and Propagation (EuCAP)*, 2020, pp. 1–5.

[72] C. Cheng and A. Zaji, "Characterization of propagation phenomena relevant for 300 GHz wireless data center links," *IEEE Transactions on Antennas and Propagation*, vol. 68, no. 2, pp. 1074–1087, 2020.

[73] C. Cheng, S. Kim, and A. Zaji, "Comparison of path loss models for indoor 30 GHz, 140 GHz, and 300 GHz channels," in *2017 11th European Conference on Antennas and Propagation (EUCAP)*, 2017, pp. 716–720.

[74] M. M. Mechaik, "Signal attenuation in transmission lines," in *Proceedings of the IEEE 2001. 2nd International Symposium on Quality Electronic Design*, 2001, pp. 191–196.

[75] A. Kavatjikidis, D. Edwards, and C. Stevens, "A long-range UWB channel sounding system exploiting UWB over fibre technology," in *Ultra-Wideband, Short Pulse Electromagnetics 9*. New York, NY: Springer New York, 2010, pp. 439–447.

[76] J. Medbo, H. Asplund, J. Berg, and N. Jalden, "Directional channel characteristics in elevation and azimuth at an urban macrocell base station," in *2012 6th European Conference on Antennas and Propagation (EUCAP)*, 2012, pp. 428–432.

[77] R. Naderpour, J. Vehmas, S. Nguyen, J. Jrvelinen, and K. Haneda, "Spatio-temporal channel sounding in a street canyon at 15, 28 and 60 GHz," in *2016 IEEE 27th Annual International Symposium on Personal, Indoor, and Mobile Radio Communications (PIMRC)*, 2016, pp. 1–6.

[78] W. Stephens and T. Joseph, "System characteristics of direct modulated and externally modulated RF fiber-optic links," *Journal of Lightwave Technology*, vol. 5, no. 3, pp. 380–387, 1987.

[79] F. Zhang, X. Ge, B. Gao, J. Wei, and S. Pan, "Phase stable radio distribution over optic cable by phase conjugation using an optical frequency comb," in *2015 International Topical Meeting on Microwave Photonics (MWP)*, 2015, pp. 1–4.

[80] M. Calhoun, S. Huang, and R. L. Tjoelker, "Stable photonic links for frequency and time transfer in the deep-space network and antenna arrays," *Proceedings of the IEEE*, vol. 95, no. 10, pp. 1931–1946, 2007.

[81] L. Novosel and G. Šišul, "Comparison of pseudo noise sequence lengths for a correlator channel sounder," in *Proceedings ELMAR-2014*, 2014, pp. 1–4.

[82] J. Kivinen, "60-GHz wideband radio channel sounder," *IEEE Transactions on Instrumentation and Measurement*, vol. 56, no. 5, pp. 1831–1838, 2007.

[83] T. S. Rappaport, S. Sun, R. Mayzus, H. Zhao, Y. Azar, K. Wang, G. N. Wong, J. K. Schulz, M. Samimi, and F. Gutierrez, "Millimeter wave mobile communications for 5G cellular: It will work!" *IEEE Access*, vol. 1, pp. 335–349, 2013.

[84] R. J. Weiler, M. Peter, T. Khne, M. Wisotzki, and W. Keusgen, "Simultaneous millimeter-wave multi-band channel sounding in an urban access scenario," in *2015 9th European Conference on Antennas and Propagation (EuCAP)*, 2015, pp. 1–5.

[85] J. D. PARSONS, D. A. DEMERY, and A. M. D. TURKMANI, "Sounding techniques for wideband mobile radio channels : a review," *IEE proceedings. I, Communications, speech, and vision*, vol. 138, no. 5, pp. 437–446, 1991.

[86] J. D. Parsons, *The mobile radio propagation channel.* John Wiley & Sons Ltd., 2000.

[87] R. J. Pirkl and G. D. Durgin, "Optimal sliding correlator channel sounder design," *IEEE Transactions on Wireless Communications*, vol. 7, no. 9, pp. 3488–3497, Sep. 2008.

[88] D. Cox, "Delay Doppler characteristics of multipath propagation at 910 MHz in a suburban mobile radio environment," *IEEE Transactions on Antennas and Propagation*, vol. 20, no. 5, pp. 625–635, 1972.

[89] C. Jansen, R. Piesiewicz, D. Mittleman, T. Kurner, and M. Koch, "The impact of reflections from stratified building materials on the wave propagation in future indoor terahertz communication systems," *IEEE Transactions on Antennas and Propagation*, vol. 56, no. 5, pp. 1413–1419, 2008.

[90] N. Vieweg, N. Krumbholz, T. Hasek, R. Wilk, V. Bartels, C. Keseberg, V. Pethukhov, M. Mikulics, L. Wetenkamp, and M. Koch, "Fiber-coupled THz spectroscopy for monitoring polymeric compounding processes," in *Optical Measurement Systems for Industrial Inspection V*, W. Osten, C. Gorecki, and E. L. Novak, Eds., vol. 6616, International Society for Optics and Photonics. SPIE, 2007, pp. 1063 – 1070.

[91] C. Ling, X. Yin, R. Mller, S. Hfner, D. Dupleich, C. Schneider, J. Luo, H. Yan, and R. Thom, "Double-directional dual-polarimetric cluster-based characterization of 70 - 77 GHz indoor channels," *IEEE Transactions on Antennas and Propagation*, vol. 66, no. 2, pp. 857–870, 2018.

[92] R. S. Thoma, D. Hampicke, A. Richter, G. Sommerkorn, A. Schneider, U. Trautwein, and W. Wirnitzer, "Identification of time-variant directional mobile radio channels," *IEEE Transactions on Instrumentation and Measurement*, vol. 49, no. 2, pp. 357–364, 2000.

[93] J. Karedal, A. J. Johansson, F. Tufvesson, and A. F. Molisch, "Shadowing effects in mimo channels for personal area networks," in *IEEE Vehicular Technology Conference*, 2006, pp. 1–5.

[94] R. Schmidt, "Multiple emitter location and signal parameter estimation," *IEEE Transactions on Antennas and Propagation*, vol. 34, no. 3, pp. 276–280, 1986.

[95] B. H. Fleury, M. Tschudin, R. Heddergott, D. Dahlhaus, and K. Ingeman Pedersen, "Channel parameter estimation in mobile radio environments using the SAGE algorithm," *IEEE Journal on Selected Areas in Communications*, vol. 17, no. 3, pp. 434–450, 1999.

[96] T. Kürner and S. Priebe, "Towards THz communications - status in research, standardization and regulation," *Journal of infrared, millimeter and terahertz waves*, vol. 35, no. 1, pp. 53–62, 2014.

[97] E. M. Vitucci, M. Zoli, F. Fuschini, M. Barbiroli, V. Degli-Esposti, K. Guan, B. Peng, and T. Kuerner, "Tri-band mm-wave directional channel measurements in indoor environment," in *2018 IEEE 29th Annual International Symposium on Personal, Indoor and Mobile Radio Communications (PIMRC)*, 2018, pp. 205–209.

[98] m. Seijo, I. Val, and J. A. López-Fernndez, "Portable full channel sounder for industrial wireless applications with mobility by using sub-nanosecond wireless time synchronization," *IEEE Access*, vol. 8, pp. 175 576–175 588, 2020.

[99] R. Zhang, S. Wang, X. Lu, W. Duan, and L. Cai, "Two-dimensional DoA estimation for multipath propagation characterization using the array response of PN-sequences," *IEEE Transactions on Wireless Communications*, vol. 15, no. 1, pp. 341–356, 2016.

[100] E. Lemos Cid, M. Garcia Sanchez, and A. Vazquez Alejos, "High speed transmission at 60 GHz for 5G communications," in *2015 IEEE International Symposium on Antennas and Propagation USNC/URSI National Radio Science Meeting*, 2015, pp. 1007–1008.

[101] T. Kleine-Ostmann, R. Piesiewicz, N. Krumbholz, D. Mittleman, T. Kurner, and M. Koch, "Characterization of building materials for the modeling of pico-cellular THz communication systems," in *2005 Joint 30th International Conference on Infrared and Millimeter Waves and 13th International Conference on Terahertz Electronics*, vol. 2, 2005, pp. 592–593 vol. 2.

[102] C. Jansen, S. Priebe, C. Moller, M. Jacob, H. Dierke, M. Koch, and T. Kurner, "Diffuse scattering from rough surfaces in THz communication channels," *IEEE Transactions on Terahertz Science and Technology*, vol. 1, no. 2, pp. 462–472, 2011.

[103] H. Zhao, L. Wei, M. Jarrahi, and G. Pottie, "Propagation measurements for indoor wireless communications at 350/650 GHz," in *2018 43rd International Conference on Infrared, Millimeter, and Terahertz Waves (IRMMW-THz)*, 2018, pp. 1–2.

[104] K. Guan, B. Peng, D. He, J. M. Eckhardt, S. Rey, B. Ai, Z. Zhong, and T. Kürner, "Channel characterization for intra-wagon communication at 60 and 300 GHz bands," *IEEE Transactions on Vehicular Technology*, vol. 68, no. 6, pp. 5193–5207, 2019.

[105] Y. He, Y. Chen, L. Zhang, S. Wong, and Z. N. Chen, "An overview of terahertz antennas," *China Communications*, vol. 17, no. 7, pp. 124–165, 2020.

[106] K. Konstantinidis, A. Feresidis, C. Constantinou, M. Gashinova, E. Hoare, M. Lancaster, and P. Gardner, "A THz dielectric lens antenna," in *2016 IEEE International Symposium on Antennas and Propagation (APSURSI)*, 2016, pp. 1493–1494.

[107] K. Konstantinidis, A. P. Feresidis, C. C. Constantinou, E. Hoare, M. Gashinova, M. J. Lancaster, and P. Gardner, "Low-thz dielectric lens antenna with integrated waveguide feed," *IEEE Transactions on Terahertz Science and Technology*, vol. 7, no. 5, pp. 572–581, 2017.

[108] S. Rey, D. Ulm, T. Kleine-Ostmann, and T. Kürner, "Performance evaluation of a first phased array operating at 300 ghz with horn elements," in *2017 11th European Conference on Antennas and Propagation (EUCAP)*, 2017, pp. 1629–1633.

[109] M. Ćwikliński, P. Brückner, S. Leone, C. Friesicke, H. Maβler, R. Lozar, S. Wagner, R. Quay, and O. Ambacher, "D-band and G-band high-performance GaN power amplifier MMICs," *IEEE Transactions on Microwave Theory and Techniques*, vol. 67, no. 12, pp. 5080–5089, 2019.

[110] A. S. H. Ahmed, M. Seo, A. A. Farid, M. Urteaga, J. F. Buckwalter, and M. J. W. Rodwell, "A 140GHz power amplifier with 20.5dBm output power and 20.8% PAE in 250-nm InP HBT technology," in *2020 IEEE/MTT-S International Microwave Symposium (IMS)*, 2020, pp. 492–495.

[111] K. Ning, Y. Fang, M. Rodwell, and J. Buckwalter, "A 130-GHz power amplifier in a 250-nm InP process with 32% PAE," in *2020 IEEE Radio Frequency Integrated Circuits Symposium (RFIC)*, 2020, pp. 1–4.

[112] E. Aguilar, A. Hagelauer, D. Kissinger, and R. Weigel, "A low-power wideband D-band LNA in a 130 nm BiCMOS technology for imaging applications," in *2018 IEEE 18th Topical Meeting on Silicon Monolithic Integrated Circuits in RF Systems (SiRF)*, 2018, pp. 27–29.

[113] D. Parveg, M. Varonen, D. Karaca, A. Vahdati, M. Kantanen, and K. A. I. Halonen, "Design of a D-Band CMOS amplifier utilizing coupled slow-wave coplanar waveguides," *IEEE Transactions on Microwave Theory and Techniques*, vol. 66, no. 3, pp. 1359–1373, 2018.

[114] P. Rodrguez-Vzquez, J. Grzyb, N. Sarmah, B. Heinemann, and U. R. Pfeiffer, "A 65 Gbps QPSK one meter wireless link operating at a 225255 GHz tunable carrier in a SiGe HBT technology," in *2018 IEEE Radio and Wireless Symposium (RWS)*, 2018, pp. 146–149.

[115] J. Tang, Z. Xu, and B. M. Sadler, "Performance analysis of b-bit digital receivers for TR-UWB systems with inter-pulse interference," *IEEE Transactions on Wireless Communications*, vol. 6, no. 2, pp. 494–505, 2007.

[116] H. Jia, X. Guo, X. Zheng, X. Xu, D. Wu, L. Zhou, J. Wu, and X. Liu, "A 4-bit 36 GS/s ADC with 18 GHz analog bandwidth in 40 nm CMOS process," *Electronics*, vol. 9, no. 10, 2020. [Online]. Available: https://www.mdpi.com/2079-9292/9/10/1733

[117] R. A. Kertis, J. S. Humble, M. A. Daun-Lindberg, R. A. Philpott, K. E. Fritz, D. J. Schwab, J. F. Prairie, B. K. Gilbert, and E. S. Daniel, "A 20 GS/s 5-bit SiGe BiCMOS dual-Nyquist flash ADC with sampling capability up to 35 GS/s featuring offset corrected exclusive-or comparators," *IEEE Journal of Solid-State Circuits*, vol. 44, no. 9, pp. 2295–2311, 2009.

[118] G. Tretter, M. M. Khafaji, D. Fritsche, C. Carta, and F. Ellinger, "Design and characterization of a 3-bit 24-gs/s flash adc in 28-nm low-power digital cmos," *IEEE Transactions on Microwave Theory and Techniques*, vol. 64, no. 4, pp. 1143–1152, 2016.

[119] L. Kull, J. Pliva, T. Toifl, M. Schmatz, P. A. Francese, C. Menolfi, M. Brndli, M. Kossel, T. Morf, T. M. Andersen, and Y. Leblebici, "Implementation of low-power 68 b 3090 GS/s time-interleaved ADCs with optimized input bandwidth in 32 nm CMOS," *IEEE Journal of Solid-State Circuits*, vol. 51, no. 3, pp. 636–648, 2016.

[120] M. Chu, P. Jacob, J. Kim, M. R. LeRoy, R. P. Kraft, and J. F. McDonald, "A 40 Gs/s time interleaved ADC using SiGe BiCMOS technology," *IEEE Journal of Solid-State Circuits*, vol. 45, no. 2, pp. 380–390, 2010.

[121] K. Guan, B. Peng, D. He, J. M. Eckhardt, S. Rey, B. Ai, Z. Zhong, and T. Kürner, "Measurement, simulation, and characterization of train-to-infrastructure inside-station channel at the Terahertz band," *IEEE Transactions on Terahertz Science and Technology*, vol. 9, no. 3, pp. 291–306, 2019.

[122] N. Khalid and O. B. Akan, "Experimental throughput analysis of low-THz MIMO communication channel in 5G wireless networks," *IEEE Wireless Communications Letters*, vol. 5, no. 6, pp. 616–619, 2016.

[123] K. N5227B. [Online]. Available: https://www.keysight.com/en/pdx-2812784-pn-N5227B/pna-microwave-network-analyzer-67-ghz?&cc=DK&lc=dan

[124] A.-I. LB-3-25-A. [Online]. Available: http://www.ainfoinc.com.cn/en/pro_pdf/new_products/antenna/StandardGainHornAntenna/tr_LB-3-25.pdf

[125] S. Jaeckel, N. Turay, L. Raschkowski, L. Thiele, R. Vuohtoniemi, M. Sonkki, V. Hovinen, F. Burkhardt, P. Karunakaran, and T. Heyn, "Industrial indoor measurements from 2-6 ghz for the 3gpp-nr and quadriga channel model," in *2019 IEEE 90th Vehicular Technology Conference (VTC2019-Fall)*, 2019, pp. 1–7.

[126] K. Guan, B. Peng, D. He, J. M. Eckhardt, H. Yi, S. Rey, B. Ai, Z. Zhong, and T. Krner, "Channel sounding and ray tracing for intrawagon scenario at mmwave and sub-mmwave bands," *IEEE Transactions on Antennas and Propagation*, vol. 69, no. 2, pp. 1007–1019, 2021.

[127] F. Sheikh, D. Lessy, and T. Kaiser, "A novel ray-tracing algorithm for non-specular diffuse scattered rays at terahertz frequencies," in *2018 First International Workshop on Mobile Terahertz Systems (IWMTS)*, 2018, pp. 1–6.

[128] D. M. Mittleman, "Twenty years of terahertz imaging," *Opt. Express*, vol. 26, no. 8, pp. 9417–9431, Apr 2018. [Online]. Available: http://www.opticsexpress.org/abstract.cfm?URI=oe-26-8-9417